Exploration and Assessment of the Environmental Design Space for Commercial Aircraft and Future Technologies

by

Garrett E. Barter

B.S., Massachusetts Institute of Technology (2002)

Submitted to the Department of Aeronautics and Astronautics
in partial fulfillment of the requirements for the degree of

Master of Science in Aeronautics and Astronautics
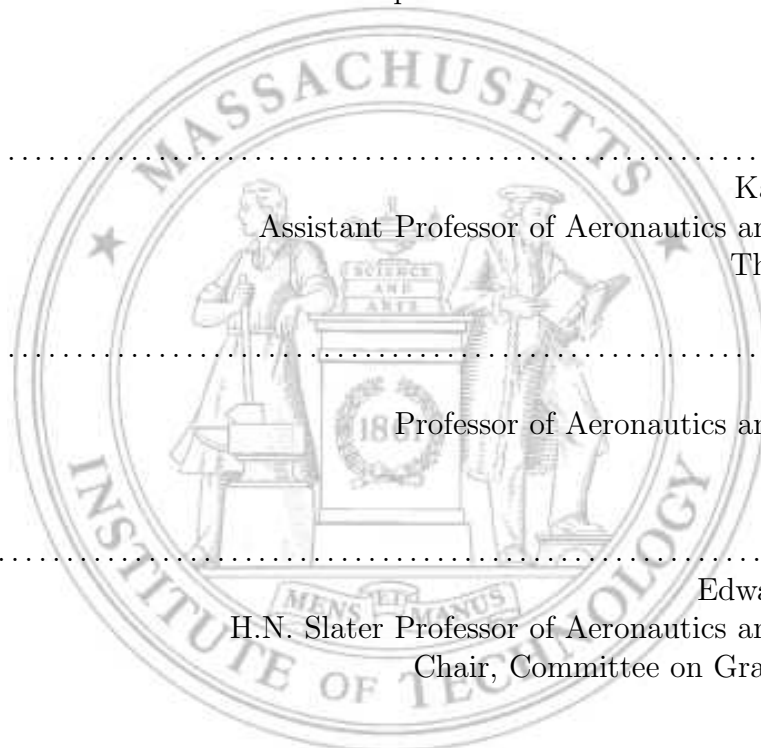
at the

MASSACHUSETTS INSTITUTE OF TECHNOLOGY

June 2004

Author . . . .
Department of Aeronautics and Astronautics
May 14, 2004

Certified by . . . .
Karen E. Willcox
Assistant Professor of Aeronautics and Astronautics
Thesis Supervisor

Certified by . . . .
Ian A. Waitz
Professor of Aeronautics and Astronautics

Accepted by . . . .
Edward M. Greitzer
H.N. Slater Professor of Aeronautics and Astronautics
Chair, Committee on Graduate Students

Exploration and Assessment of the Environmental Design Space for Commercial Aircraft and Future Technologies

by

Garrett E. Barter

Abstract

Design and regulatory initiatives for aircraft noise and emissions should appreciate the integrated nature of the aircraft system. The computational ability exists to consider environmental and traditional performance objectives of aircraft concurrently. This context of multi-disciplinary system design is named the Environmental Design Space (EDS) and is studied in this thesis with an integrated aircraft-engine conceptual design framework. With this tool, the objectives of this thesis were to assess the fidelity and level of uncertainty of the design framework, to characterize the tradeoffs between aircraft noise, emissions and aircraft performance and to evaluate the system-level impacts of a future noise reduction technology.

Assessment of the EDS framework was accomplished with a probabilistic model assessment methodology. The assessment involved the selection of stochastic inputs and generation of output distributions through Monte Carlo simulations. A sensitivity analysis of the key drivers of uncertainty and the user-defined input distributions is also provided. This methodology was applied to one of the framework modules, the NASA Engine Performance Program (NEPP), and found that the modeling error was subsumed within the modeling uncertainty. A sensitivity study indicated that the component efficiencies had the largest impact on the output distribution. When the level of NEPP uncertainty was propagated to the system level, the resulting coefficient of variance for fuel burn was 4.1%.

The tradeoffs between the competing EDS objectives were characterized through Pareto fronts generated by multi-objective genetic algorithms. The quantification of these trades for a given aircraft, $8\,dB$ in cumulative EPNL vs. $8\,kg$ of $LTO\text{-}NO_x$ for example, give designers and regulators supporting information for their decisions. A future noise reduction technology, fan trailing edge blowing, was also evaluated at the system level. A probabilistic analysis of the technology design in the EDS framework revealed poor tolerance of engine cycle variability. A robust design procedure was employed, and showed that while the technology offered a flyover noise reduction of $11.9\,dB$, it incurred a fuel burn and $LTO\text{-}NO_x$ penalty of 2.8% and 11.0%, respectively.

Thesis Supervisor: Karen E. Willcox
Title: Assistant Professor of Aeronautics and Astronautics

Acknowledgments

I owe an enormous debt of thanks to those that have helped me complete this thesis and to those that have helped me reach this accomplishment in general.

First, this work would not have been possible without the technical expertise and support of my advisor, Prof. Karen Willcox. I have come to greatly respect her keen insight into complex problems and have enjoyed building this project with her. I would also like to thank Prof. Ian Waitz whose experience and guidance on research and environmental issues has proved invaluable. I have learned many invaluable lessons from both of them and appreciate the high standards they have held me to. Thanks also to the Stanford EDS crew, Prof. Ilan Kroo and Nicolas Antoine, for their collaboration on the project and support with the use of Caffe. I would be remiss to not give credit to Victor Garzon, whose research established many of the implementations and know-how of the methods that I used. His groundwork has spared me from the pains and anguish of re-inventing the wheel many times over. Finally, the conversations and advice from Jeff Berton, Sean Bradshaw, Prof. David Darmofal, Yann Deremaux, Prof. Dan Frey, Karl Geiselhardt, Prof. Edward Greitzer, Joe Lee, Stephen Lukachko, Alexis Manneville, Arnie McCullers, Deborah Pilczer, John Rawls, Vince Sidwell, Chris Snyder, Prof. Zoltan Spakovszky and Mike Tong all proved crucial at various points in the research. I apologize that I could not be more personal in my gratitude.

On a personal note, I certainly would not have survived another two years at MIT without the camaraderie of the other students in ACDL and my roommates at the FunkP. I would like to make special mention and thanks to Elke, with whom I have grown and shared so much that I can only hope to continue growing and sharing for a long time to come. Finally, I of course would like to thank my family for everything they have given me and always providing me with the independence and support in whatever I do, even during especially difficult times. Mom, Dad, Mickey and Devra- I love you all very much.

Contents

List of Figures

List of Tables

Nomenclature

ANOPP	Aircraft Noise Prediction Program
AR	Aspect ratio
BPF	Blade Passing Frequency
BPR	Bypass ratio
CV	Coefficient of Variation
EPNL	Effective perceived noise level
DOC	Direct operating cost
FAA	Federal Aviation Administration
FAR	Federal Aviation Regulation
FPR	Fan pressure ratio
GA	Genetic algorithm
GEAE	General Electric Aircraft Engines
GTOW	Gross takeoff weight
h	Flight altitude
HPC	High Pressure Compressor
HPT	High Pressure Turbine
HSCT	High Speed Civil Transport
IOC	Indirect operating cost
LPC	Low Pressure Compressor
LPT	Low Pressure Turbine
$LTO\text{-}NO_x$	Nitrous oxides emitted during landing-takeoff cycle
NEPP	NASA Engine Performance Program
NO_x	Nitrous oxides
OPR	Overall pressure ratio
PASS	Program for Aircraft Synthesis Studies
PDF	Probability density function
PNL	Perceived noise level
P&W	Pratt & Whitney
SAE	Society of Automotive Engineers
RSM	Response Surface Methodology
SBJ	Supersonic Business Jet
SFC	Specific fuel consumption
SLS Thrust	Sea-level static thrust
SPL	Sound pressure level
S_{ref}	Wing surface area
t/c	Wing thickness-to-chord ratio
TSFC	Thrust specific fuel consumption
TOC	Total operating cost
T_{t4}	Turbine inlet total (stagnation) temperature
UCAV	Uninhabited Combat Aerial Vehicle

Chapter 1

Introduction

1.1 Motivation

Commercial aircraft contribute to both noise and emissions pollution on a local and global scale. Although initially considered side-effects, eventually efforts arose to reduce the environmental impact of aircraft. Neighborhoods near airports grew annoyed with the noise disturbances and health concerns over local air quality, from all industrial pollutants, culminated in the Clean Air Act of 1970. Regulatory agencies and the influx of new technologies both steered aircraft development towards a mitigation of noise and emissions. Improved combustors and the turbofan engine were important parts of this progress.

During the time of noise and emissions regulation, the two outputs have been addressed separately from one another. Meaning, the regulatory decisions for noise standards had no bearing on the regulatory decisions for emissions standards. Regulatory agencies did recognize that both noise and emissions concerns impact aircraft performance. For instance, higher temperatures of compressor exit temperatures improve the thermodynamic efficiency of the engine cycle, but also augment the production of nitrous oxides, NO_x. Similarly, quiet engine designs seek to maximize the bypass ratio of the engine, but an excessive BPR also compounds nacelle drag and degrades aircraft performance. This twofold approach to noise and emissions concerns can be improved. Aircraft-engine designs have evolved to a point where noise and emissions performance not only impact fuel economy, but also each other. Any future, aggressive emissions reduction will impose penalties for fuel efficiency as well as noise, and vice-versa. Additionally, as aircraft-engine designs have evolved, regulations for both noise and emissions have also become more stringent. As this trend continues, regulators must be cognizant that noise and emissions can no longer be regulated independent of one another.

The multi-disciplinary, aircraft-engine system design for both environmental and
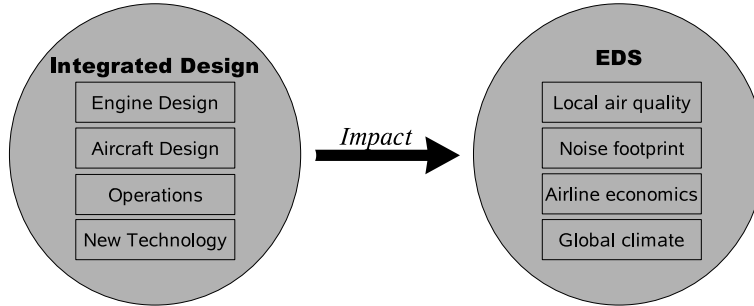
Figure 1-1: Integrated aircraft-engine-operations tool allows for environmental design space exploration and evaluation within the larger air transportation system.

traditional aircraft performance is designated as the *Environmental Design Space* (EDS). This novel approach gives consideration to both airline and environmental interests. In this setting, future aircraft-engine designs, new technologies and operational modifications can be evaluated and weighted between the various EDS objectives. This allows both designers, operators and regulators to understand and appreciate the inherent tradeoffs involved in the aircraft system. Current tools capable of exploring EDS are proprietary and are too focused on either the airframe or the engine. Additionally, the stakeholders interested in the implications and tradeoffs of EDS include aircraft manufacturers, airlines, regulatory agencies, local airports, academia and governmental officials. Each of these stakeholders has its own interests and concerns for environmental trades of aircraft. Thus, an open source tool that is accepted by all stakeholders is necessary to collectively advance the state-of-the-art in aircraft design. This tool must be an integrated aircraft-engine design tool that has the capability of capturing the broader air transportation system at the airline fleet and operations level, yet flexible enough to model new technologies.

Conceptual design tools capable of satisfying the requirements for EDS exploration are complex, modular and multi-disciplinary. Each of the components of the tool has its own approximations and modeling assumptions. When the modules interact to predict aircraft noise, emissions or performance, their approximations and assumptions stack up on one another, creating uncertainty. Since the framework for EDS exploration is intended to give the various stakeholders information by which to make decisions, understanding the system level uncertainty of the tool is an important element of the research. This understanding begins with an assessment of each module by itself and a propagation of individual module uncertainty to the system level.

1.2 Thesis Objectives

The primary objectives of this thesis are:

- Devise a generic process for model assessment of complex design tools and apply that process to a sample module.

- Use an integrated, aircraft-engine preliminary design tool to characterize the tradeoffs between noise, emissions and aircraft performance.

- Evaluate the tradeoffs and aircraft system-level impacts of a future noise reduction technology.

Since the prediction of environmental performance, future designs and regulatory trends are uncertain, a probabilistic approach is taken whenever possible for all of the above objectives.

1.3 Previous Work

Model assessment has caught the attention of many researchers for many years. The prominent use of computational tools for scientific and engineering applications has given popularity to this topic [16]. Unfortunately, there is no universally accepted basis for assessment. However, some professional societies provide guides for *verification* and *validation* (V & V) of computational models [2, 11, 41]. Validation speaks to the correctness of the translation of the physical world to the fundamental model, while verification alludes to the correctness of the translation of the model to the computer implementation [2, 6, 47]. Additionally, the emergence of probabilistic methods has brought appreciation for the notion of uncertainty in assessment studies with particular emphasis on the disparity between *error* and *uncertainty* [2, 6, 38, 45]. Probabilistic model assessment has been considered and discussed previously by Baghdasaryan et al. [6], but the efforts in this thesis extend this work considerably. Additional discussion can be found in Chapter 4.

Research related to EDS has been conducted by both industry and academia. At GEAE, their PREDATER (Preliminary Robust Engine Design Analysis Tool for Evaluating customer Return) tool combines noise, emissions and cost predictions into a preliminary engine design code [49]. This tool allows for trades within the environmental design space specifically for large commercial engines. The trades are made for candidate conceptual designs and the inclusion of new technologies. By including a cost model, PREDATER frames all tradeoffs and decisions as cost-benefit scenarios. By expressing design variables as stochastic, it also allows for probabilistic and robust analyses. However, the GEAE PREDATER tool is proprietary and ignores the role of the aircraft.

Many EDS related studies have been performed by the Aerospace Systems Design Laboratory at Georgia Tech. DeLaurentis, Roth and Mavris have utilized probabilistic methods for preliminary aircraft and engine design. Roth and Mavris sized engines for an Uninhabited Combat Aerial Vehicle (UCAV) and commercial aircraft applications through the use of RSMs, while DeLaurentis and Mavris used a related approach for aircraft [10, 29, 31, 36, 37]. These probabilistic conceptual design studies included some EDS metrics, such as fuel burn and noise, but did not directly address their tradeoffs. Briceño and Mavris did offer a conceptual design space exploration for a supersonic business jet through a RSM for noise, emissions and fuel efficiency [8]. However, their research, like many of the above Georgia Tech papers, did not delve deeply into the physical processes that drove the results. Kirby and Mavris have devised an algorithm for technology impact forecasting and decision making. This algorithm has been applied to a few example cases, such as a High Speed Civil Transport (HSCT), an UCAV and a turbofan engine [22, 30, 32, 35]. While these investigations do not address the environmental design space directly, they do treat future technologies as uncertain and conduct their analysis via probabilistic means. For all of the above publications, with the exception of the study by Briceño and Mavris, emissions was not an output metric of interest. Additionally, almost all of the investigations relied upon RSM for analysis, which can overly simplify the physical interactions at play in an aircraft-engine system [13, 45].

Much of the groundwork for this research has been laid by Antoine and Kroo. They have performed optimizations of large commercial aircraft for minimum environmental impact [4, 5, 26]. Through these optimizations they examined the tradeoffs between noise performance, operational considerations and relative cost. For instance, to accomplish a specified noise reduction for a reference aircraft, the optimizations pointed to a an aircraft with a higher AR and larger BPR to fly at a lower cruise altitude with greater installed thrust and a 1% operating cost penalty. The optimizations did not focus solely on aircraft design, however. A parametric investigation into operational modifications, such as steeper approaches and takeoff thrust cutback, was also performed and indicated great promise for noise reduction. This research provided the infrastructure of experience and computational tools upon which this thesis was built. The Stanford studies employed an integrated aircraft-engine design framework, as illustrated in Figure 1-2, that was later adopted for use in this thesis.

1.4   Outline

This thesis presents an initial characterization of the environmental design space, the model used for its analysis and the means to assess complex design tools. This chapter has introduced the concept of EDS and provided a survey of previous, related research.
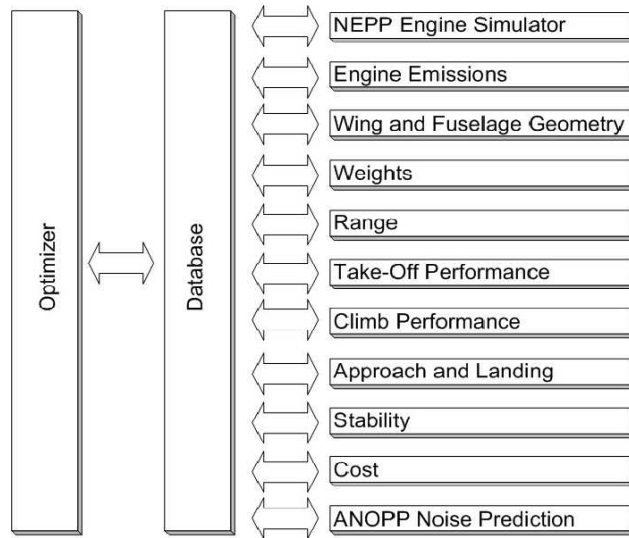
Figure 1-2: Flowchart depiction of Stanford computational framework [4].

Chapter 2 supplies an overview of the numerical techniques and environmental metrics used in all of the studies for this thesis. This is followed by a detailed description of the EDS framework, its modules and the motivation for using an integrated aircraft-engine design tool in Chapter 3. Chapter 4 elicits a preliminary assessment of the design tool by developing a probabilistic model assessment methodology and applying it to one of the modules. Chapter 5 begins to establish the tradeoffs between multiple EDS metrics and also offers a system-level assessment of a future noise reduction technology within the context of EDS. The thesis ends with Chapter 6 recapitulating the key points and suggesting pathways of future development.

It should be noted that for all of the investigations in Chapters 3 & 5, the baseline aircraft was a 275 passenger wide-body aircraft. This size, approximately the same as a Boeing 767-300ER, was selected because of its similarity to the next generation Boeing aircraft, the 7E7.

Chapter 2

Numerical Approach

2.1   Introduction

This chapter provides the theoretical and numerical underpinnings of the tools and analyses in this thesis. All of the computational investigations of Chapters 4–5 involve either optimization or Monte Carlo simulations. These methods, and the specifics of their implementation, are described in detail. This is followed by an explanation of the noise and emissions metrics that are used in the studies.

2.2   Optimization Overview

All numerical optimizations can be framed in the same mathematical context: Using the design vector, $\mathbf{x} \in \mathbb{R}^n$, minimize the objective function, $\mathbf{J}(\mathbf{x}) \in \mathbb{R}^z$, subject to the constraints $\mathbf{g}(\mathbf{x}) \in \mathbb{R}^m$, where $\mathbf{x}$ has lower and upper bounds. Mathematically,

$$\min \mathbf{J}(\mathbf{x}) \qquad \text{s.t.} \begin{cases} \mathbf{g}(\mathbf{x}) \leq 0 \\ x_{i,LB} \leq x_i \leq x_{i,UB} \end{cases}$$

$$\begin{aligned} \text{where} \quad \mathbf{J} &= \left[J_1(\mathbf{x}) \dots J_i(\mathbf{x}) \dots J_z(\mathbf{x})\right]^T \\ \mathbf{x} &= \left[x_1 \dots x_i \dots x_n\right]^T \\ \mathbf{g} &= \left[g_1(\mathbf{x}) \dots g_i(\mathbf{x}) \dots g_m(\mathbf{x})\right]^T \end{aligned}$$

where $J_i(\mathbf{x})$ is the i-th of z objective functions, $g_i(\mathbf{x})$ is the i-th of m constraints and $\mathbf{x}$ has dimension, n.

There are a number of algorithms that can be used to solve the above optimization problem. The most popular methods are search algorithms, gradient based algorithms and heuristics. In this thesis, all optimizations were either performed with a Nelder-

Meade simplex algorithm or a genetic algorithm (GA).

2.2.1   Nelder-Meade Simplex

The Nelder-Meade simplex algorithm is intended to seek out minima of a complex design space. It should not be confused with the simplex approach to linear programming. For a design vector, $\mathbf{x} \in \mathbb{R}^n$, a *simplex* refers to the meeting of $n+1$ observation points at a convex hull [48]. In two dimensions, the simplex is the convex hull of the equilateral triangle. In three dimensions, the simplex is the convex hull of a tetrahedron. In every iteration, the optimizer starts and ends at a simplex by always moving to better performing vertices. The motion is always from one observation point vertex to a reflection vertex and does not require the computation of gradients [7]. A 2-D example is shown in Figure 2-1a. The worst performing point, 1 is reflected about the opposite side to form another equilateral triangle, thereby moving in a direction that minimizes the objective. The search continues as in Figure 2-1b. The objective is evaluated at point 4 and is shown to be the worst performing vertex of triangle 234. A reflection back to point-1 would initiate an oscillation mode, so point-2 is reflected instead. This continues until one vertex, point-16, is used repeatedly. In this case, the size of the equilateral triangles is reduced and the process repeats itself. The Nelder-Meade algorithm also allows for expansion and contraction of the simplex to expedite the search [1].

The Nelder-Meade simplex algorithm is intended for unconstrained minimization problems. The implementation of the simplex algorithm used in this thesis had to handle constraints. Instead of using a penalty function, a *better* vertex was defined as the vertex with the lowest objective function if all constraints were satisfied or the lowest cumulative percentage constraint violation if applicable. In that way, the algorithm always first sought to satisfy the constraints and then afterwards seek out the objective minimum in the feasible design space.

2.2.2   Genetic Algorithms

Genetic algorithms are a type of heuristic optimization, and therefore do not use gradients to determine search directions. GAs have their methodology origins in species evolution and the Darwinian concept of *survival of the fittest*. GAs randomly seed the design space with a population of starting designs. Population sizes are usually in the hundreds, but can be in the thousands for more complex optimizations. The design variables are encoded, as if they were DNA genes on a chromosome. In each iteration, or generation, two points are selected and *mated* together to produce child-points. A handful of mating schemes exist and their selection is the option of the designer. Usually, the parents and children are evaluated against one another in some
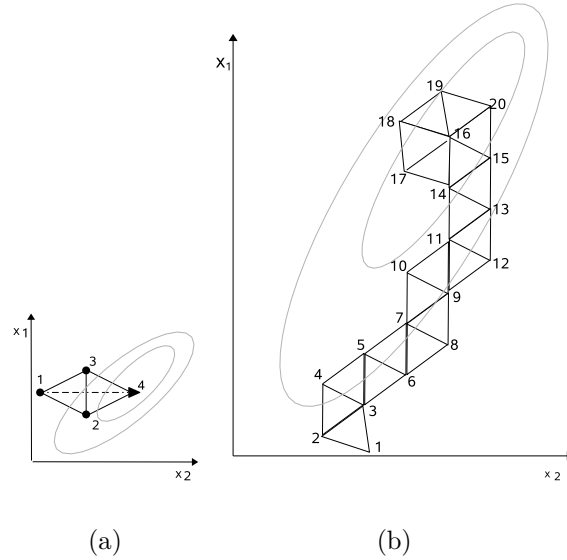
Figure 2-1: Simplex search algorithm in 2-D showing reflection of the worst performing point [1].

measure of fitness weighing the objective and constraints. Aside from the random seeding of the initial population, randomness also enters a GA through mutations, where genes are altered with a specified probability. This randomness allows GAs to escape the trappings of local minima and continue to seek out better designs. After many generations, the points should converge towards an optimal solution.

The studies in this thesis for which GAs were applied were for the generation of *Pareto fronts* through multi-objective optimization. A Pareto front depicts the tradeoffs between two or more competing objectives, as in Figure 2-2. The population basis of GAs lends itself well to Pareto fronts in a complex design space. The Pareto front itself is defined by the non-dominated, or *Rank-1* designs of the population. Non-dominated designs imply that there is no other point that performs better on all axes. For a given Rank-1 point in Figure 2-2, any other point that performs better in J_1 performs worse in J_2 and vice-versa.

The two-dimensional GA optimizations in this thesis used a population size of 500 and followed the flowchart of Figure 2-3. In every generation, every member of the population selects a mate at random and produces two offspring. The design variables of these offspring are linear combinations of the design variables of the parents, with a mutation rate of 3%. Meaning, at an occurrence frequency of 3%, a random perturbation based on the design variable upper and lower bound is applied. The fitness of the two children is evaluated and they are then added to the candidate population
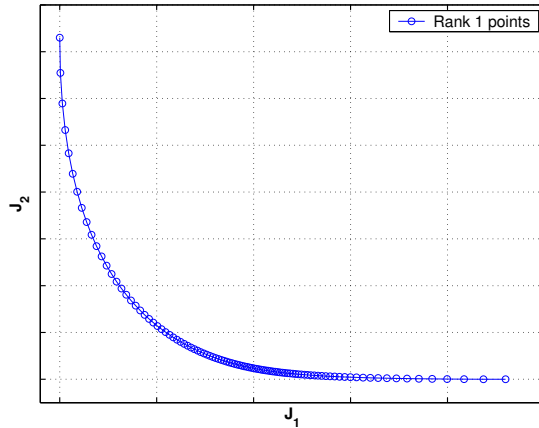
Figure 2-2: Pareto front of non-dominated designs for bi-objective optimization of J_1 and J_2.

for the next generation. With every population member producing two children the candidate population becomes three times its nominal size. The fitness is a sum of the scaled objectives and the percentage violation of all constraints multiplied by a penalty function. The applications in this thesis scaled all objectives to be $\mathcal{O}(10^2)$ and applied a penalty multiplier of 10^4 to the sum of all percentage constraint violations. Finally, the entire candidate population is ranked. This ranking is modified slightly by a measure of the distance of a candidate population member to its neighbor (niching). This ensures sufficient spread amongst the population so that the Pareto front does not cluster around one region. If the modified ranking of the best performing child is lower than the modified rank of the worst performing parent, then that parent is replaced in the population.

2.3   Monte Carlo Simulations Overview

Monte Carlo simulations are the standard approach to propagating stochastic inputs through non-linear computational models. Due to the complexity of design tools, often times output distributions cannot be explicitly expressed as functions of the input distributions. Instead, a Monte Carlo simulation constructs the output distributions empirically, one point at a time. The entire process is depicted graphically in Figure 2-4 and described in the following subsections. Greater detail on Monte Carlo simulations can be found in [15].
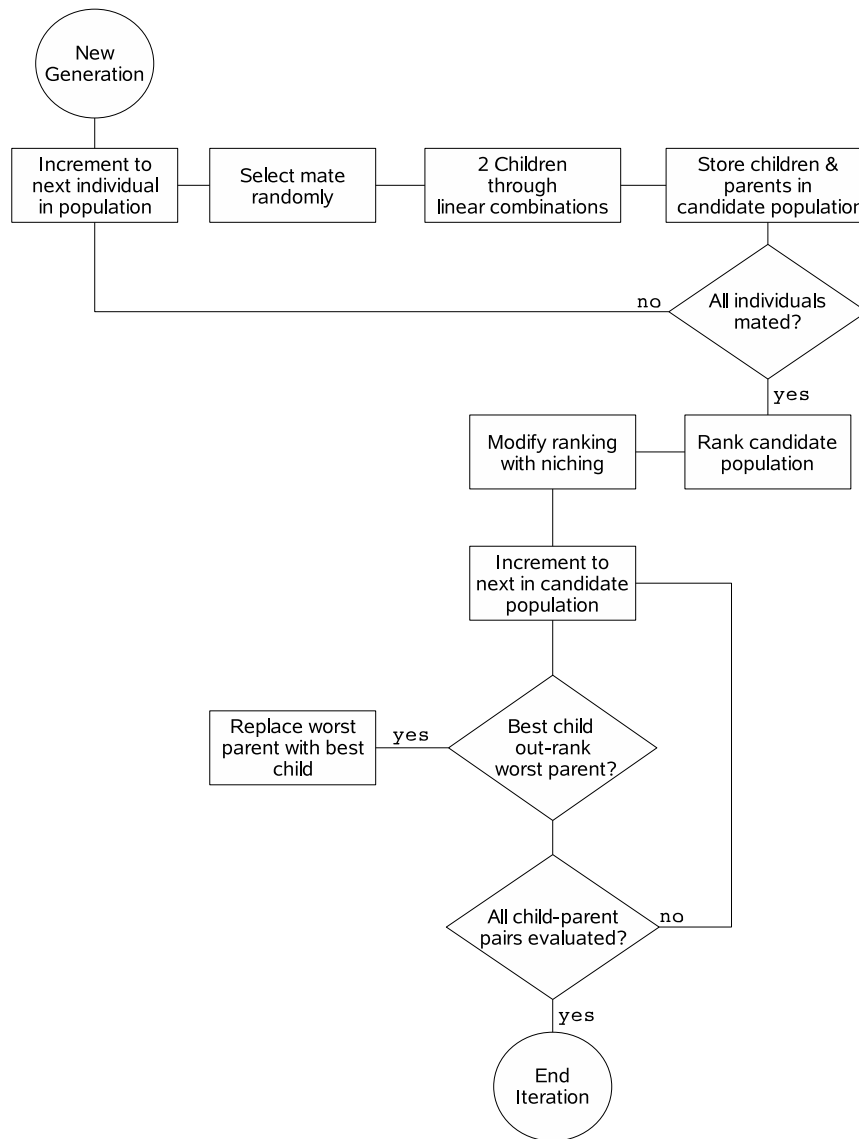
Figure 2-3: Flow chart of multi-objective genetic algorithm implementation.
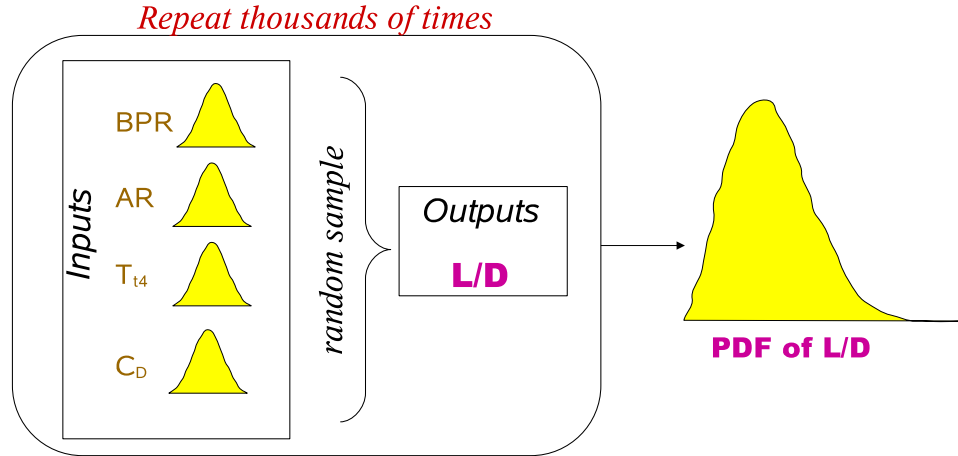
Figure 2-4: Graphical illustration of Monte Carlo simulation.

2.3.1   Constructing the Output Metrics

A Monte Carlo simulation is comprised of hundreds or thousands of single deterministic analyses. During each iteration, the probabilistic inputs are sampled from their distribution and an output is generated. Together, all of the deterministic iterations contribute to a histogram of the output metric of interest. As the number of Monte Carlo iterations grows, the output histogram approximates a probability density function (PDF).

2.3.2   Input Distributions

Monte Carlo simulations allow for all varieties of distributions for the stochastic inputs. Analytical, common PDFs can be generated by many computational tools or an empirically based PDF can be utilized instead. If the inputs are assumed independent, then with each iteration the inputs are randomly sampled separate from one another. If the inputs are correlated, and therefore not independent, then a modified sampling scheme is utilized. In the Monte Carlo simulations in this thesis, all probabilistic inputs were assumed to be independent, normally distributed random variables since they represented *uncertainty in knowledge*. Meaning, the stochastic variables were simply unknown so probability was allocated symmetrically about its mean value. Nevertheless, the methodology could be applied to general distributions.

2.3.3 Convergence

Monte Carlo simulation convergence criterion is similar to the convergence of other computational tools. Usually convergence implies reducing a residual of an equation below some threshold. However, in Monte Carlo simulations there is no governing equation or residual to drive down. Instead, with each iteration there is a new population mean and standard deviation. As the number of iterations tends towards infinity, the mean and standard deviation of the population approach their true values. Thus, the mean and standard deviation are random variables too. After any iteration, the population mean and standard deviation approximate their true values within some confidence band. If the confidence band is sufficiently small, within some tolerance, then the Monte Carlo simulation is considered converged. Mathematically, the unbiased mean and standard deviation of a sample size population can be defined as,

$$\bar{x} \;=\; \frac{1}{n}\sum_{i=1}^{n} x_i \tag{2.1}$$

$$s \;=\; \sqrt{\frac{1}{n-1}\sum_{i=1}^{n}(x_i - \bar{x})^2} \tag{2.2}$$

where $\bar{x}$ is the mean, s is the standard deviation and n is the size of the population. The $1-\alpha$ confidence intervals (where $\alpha = 0.05$ for a 95% confidence interval) of the true mean and standard deviation are given by the following equations,[15]

$$\langle\mu\rangle_{1-\alpha} \;=\; \left[\bar{x} - t\!\left(1 - \frac{\alpha}{2}\middle|n-1\right)\frac{s}{\sqrt{n}}; \;\; \bar{x} + t\!\left(1 - \frac{\alpha}{2}\middle|n-1\right)\frac{s}{\sqrt{n}}\right] \tag{2.3}$$

$$\langle\sigma\rangle_{1-\alpha} \;=\; \left[s\sqrt{\frac{n-1}{\chi^2\!\left(1 - \frac{\alpha}{2}\middle|n-1\right)}}; \;\; s\sqrt{\frac{n-1}{\chi^2\!\left(\frac{\alpha}{2}\middle|n-1\right)}}\right] \tag{2.4}$$

where:

$\langle\mu\rangle_{1-\alpha}$ $= 1-\alpha$ confidence interval for the mean
$\langle\sigma\rangle_{1-\alpha}$ $= 1-\alpha$ confidence interval for the standard deviation
$t(\cdots|n-1)$ $=$ inverse CDF of Student's t-distribution, $n-1$ degrees of freedom
$\chi^2(\cdots|n-1)$ $=$ inverse CDF of chi-square distribution, $n-1$ degrees of freedom

2.4 Acoustic Metrics

The human ear is capable of perceiving sound generation from pressure perturbations in the frequency range of 2×10^{-5}–10^3 Pa. The large range of both perceivable frequencies and pressure variations gives rise to a logarithmic scaling of loudness. The sound pressure level (SPL) is a function of frequency and is defined by,[34]

$$SPL\left(f\right) = 10\log\left(\frac{p\left(f\right)}{p_0}\right)^2 = 20\log\left(\frac{p\left(f\right)}{p_0}\right)$$

where the reference pressure, $p_0 = 2 \times 10^{-5}$. The sensitivity of the human ear to some frequencies more than others has led to the division of frequency spectra into bands and the creation of frequency weighting curves. Weighting curves are essentially filters in the frequency domain, the most common of which are called A, B, C and D. The noise analyses in this thesis relied upon a section of the 1/3 octave band spectra with center frequencies ranging from 50 Hz–10 kHz. Another metric, perceived noise level (PNL) weights frequencies that were determined to be the most *annoying* to the human ear [33]. For aircraft noise measurements, it was necessary to rely not only upon PNL, but also to account for the duration of a noise event. Thus, the effective perceived noise level (EPNL) metric was created an as adaptation of PNL [21].

The three Federal Aviation Regulation (FAR) Part 36 certification points are the standard for aircraft noise regulation. It should be noted that they do not necessarily capture the noise footprint of aircraft. Nevertheless, for consistency, the studies in this thesis relied upon these points. Noise certification is done through microphone measurements at three locations in the landing-takeoff cycle, as seen in Figure 2-5. Underneath the landing profile is the *approach* certification point and on takeoff there is an overhead, *flyover* point and a community *sideline* point. *Cumulative EPNL* refers to the summation of all three certification points and is the metric most often used in this thesis.

2.5 Emissions Metrics

Just as the noise metrics used for analysis resembled the FAR Part 36 regulations, the emissions modeling resembled the International Civil Aviation Organization (ICAO) standard procedure for measuring engine emissions. ICAO regulations are concerned with local air quality, as opposed to global climate change, and therefore focus on emissions output during the landing-takeoff (LTO) cycle. The regulations assume thrust levels and times for the various legs that comprise the LTO cycle, as depicted in Figure 2-6. For each thrust setting on an engine, an emissions index, (EI) is calculated for a particular species. From that EI and the total duration of the segment,
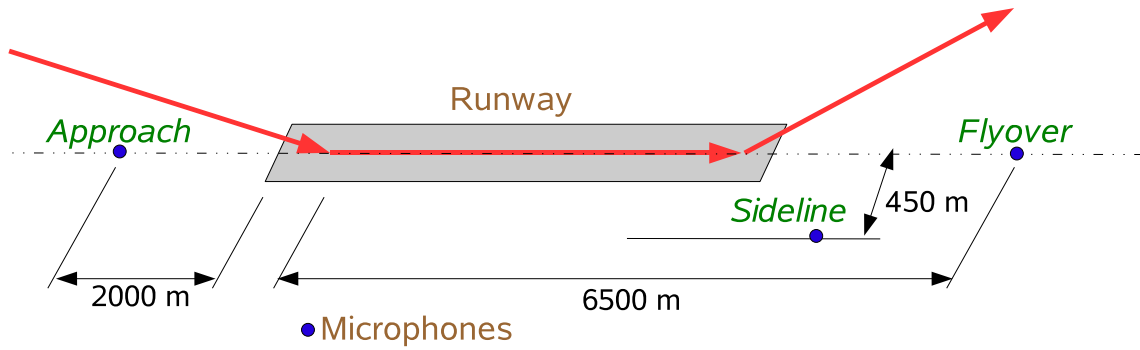
Figure 2-5: FAR 36 measurement locations for aircraft noise regulations.
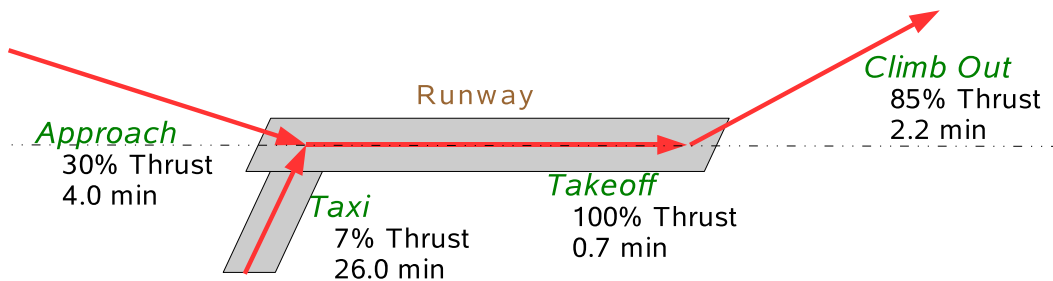
Figure 2-6: Assumed thrust settings and segment times for ICAO emissions regulations.

a total emissions output for a species can be found in kilograms. It should be noted that when agencies certify an engine for emissions, three independent experimental measurements are made for each species. There is a notable standard deviation between the three tests. Computational correlations for emissions are based on curve fits of this experimental data and only compound the uncertainty of the experimental estimates.

Chapter 3

Description of EDS Framework

3.1   Introduction

This chapter provides a detailed description of the computational framework used for EDS exploration. An overview of the tool is followed by more specific discussion of its components. Special attention is given to the NASA codes in the framework as they are directly tied to the estimations of noise and emissions. The chapter concludes with an example case study using this integrated aircraft-engine design framework.

3.2   EDS Framework Overview

The computations, optimizations, analyses and studies done for this project were all completed using the Collaborative Application Framework for Engineering (Caffe). Caffe is a database manager with systems analysis capabilities wrapped around the Program for Aircraft Synthesis Studies (PASS) and two NASA codes. PASS is a preliminary aircraft design and performance analysis tool, originally developed at Stanford. It is composed of various modules for the different aspects of aircraft design and performance evaluation, depicted graphically in Figure 3-1a. The analysis modules are grouped as shown in Figure 3-1b, either as a piece of the original Stanford PASS system or as a NASA code. The PASS routines focus on aircraft performance and have their origins in the Boeing Company, McDonnell Douglas or Stanford. The two NASA codes are the *NASA Engine Performance Program* (NEPP), which serves as the engine cycle deck, and the *Aircraft Noise Prediction Program* (ANOPP) which is utilized for noise calculations.

   The approximate methods of the PASS and NASA modules in Caffe make them ideal for the use in optimization and probabilistic analysis. Their quick execution facilitates exploration of the design space in a thorough and timely manner. The enumeration of design variables, objectives and constraints is performed through an
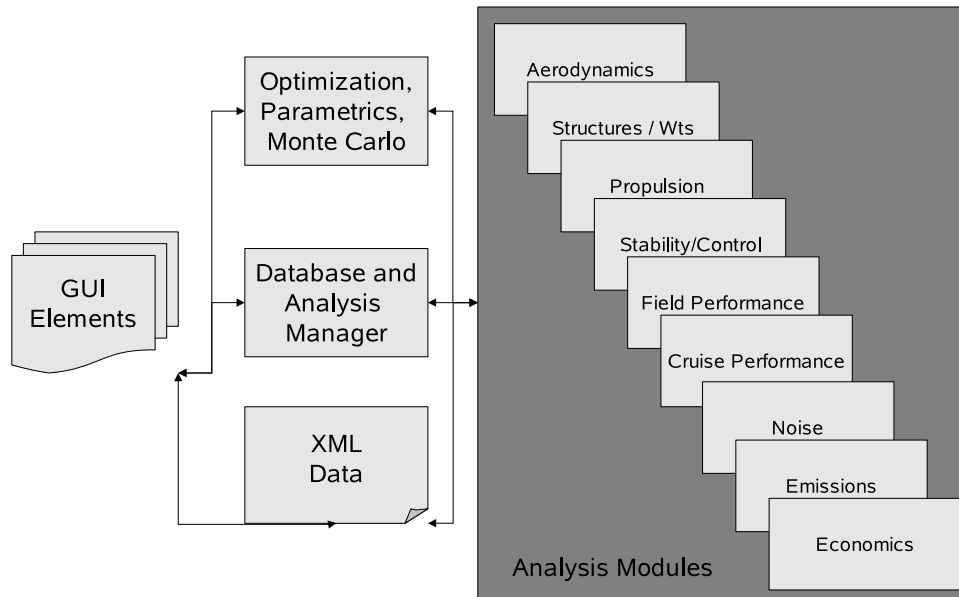
(a) Analysis modules feed into a database manager and can be run with optimizations or probabilistic evaluations [25].
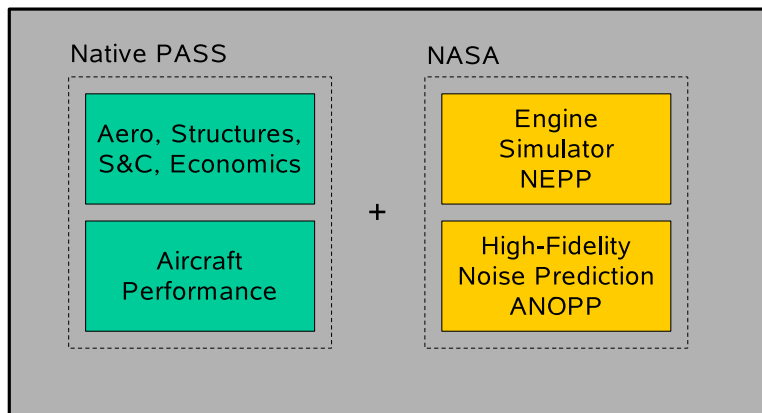
(b) Module grouping as either part of the Stanford PASS system or as a NASA program [3].

Figure 3-1: Block diagram depiction of Caffe where analysis modules represent the elements of preliminary aircraft design.

Table 3.1: Design variables, parameters, constraints and objectives for Caffe.

Design Variables	Constraints	Parameters	Objectives
Takeoff Weight	Cruise Range	No. Passengers	Est. ticket price
Wing Area	Climb Gradient	Number of Engines	Fuel Burn
Wing Aspect Ratio	Stability Margin		Takeoff Weight
Wing Sweep	C_L Wing		
Thickness:chord	C_L Tail, Takeoff		
Wing X-Position	C_L Tail, Cruise		
Horizontal Tail Area	C_L Tail, Landing		
Initial Cruise Altitude	Fuel Capacity		
Final Cruise Altitude	Takeoff Field Length		
Sea Level Static Thrust	Landing Field Length		
Bypass Ratio	Drag/Thrust		
Overall Pressure Ratio	Wing Span		
Turbine Inlet Temp	Landing Mach No		
Initial Cruise Mach	Cumulative EPNL		
Final Cruise Mach	$LTO\text{-}NO_x$		

XML-based interface, allowing for rapid changes. An extensive, but not exhaustive, list of design variables, constraints, parameters and objectives in Caffe is given in Table 3.1. Objective functions could be direct operating cost (DOC), gross takeoff weight (GTOW), range, fuel burn or another aircraft design metric. Environmental metrics could be objectives, or also constraints, thereby driving designs towards a *quiet* or *clean* aircraft. Design variables include aircraft and wing geometry description, engine cycle definition and cruise altitude selection. The flexibility of the framework enables new design variables to be easily added or removed. Parameters are chosen by the designer and are not varied or controlled by the optimizer.

3.2.1 Analysis Capabilities in Caffe

Figure 3-1a illustrates how the modules in Caffe tie into the database manager and the optimizer. There are currently two different classes of optimizers available in Caffe. The simplest and most ordinary is the *simplex* search algorithm, while GAs can also be employed. Moreover, in addition to the use of optimizers, a probabilistic capability exists in Caffe for modeling input variables as stochastic and performing Monte Carlo simulations. These analysis approaches were described in greater detail in Sections 2.2–2.3.
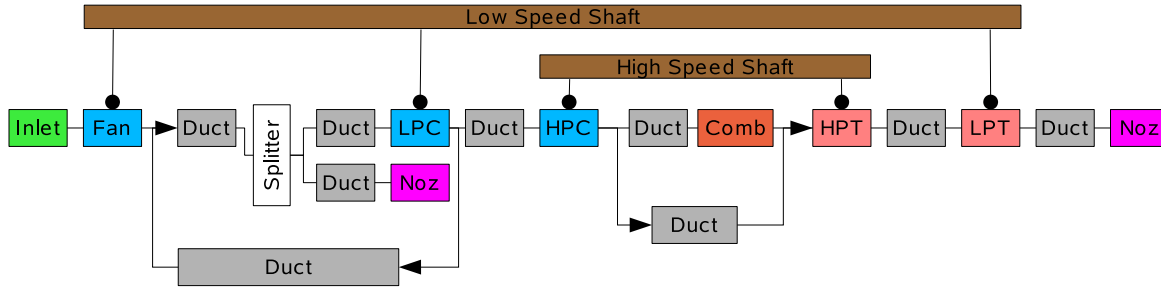
Figure 3-2: Separate-flow turbofan components used in NEPP. Adapted from [3].

3.3 Caffe Modules

This section delves deeper into the modules of Caffe that are the most closely tied with noise and emissions prediction. The NASA codes, NEPP and ANOPP, are complex software tools in their own right and are discussed at greater length below. A rigorous assessment of NEPP and its uncertainty is presented in Section 4.3, while ANOPP assessment is given below in Section 3.3.4. Since NO_x emitted during the landing-takeoff cycle ($LTO\text{-}NO_x$) is used frequently in this thesis as a metric of comparison, an overview of the emissions module is also presented.

3.3.1 The Engine Cycle Deck Module, NEPP

The NASA Engine Performance Program is a NASA code originally developed in conjunction with the Navy in the 1970s to predict the performance of military aircraft engines. Since its original development, NEPP has grown in scope and capability. It is a 1-D, steady thermodynamics analysis program capable of analyzing turbojets, turbofans, turboshafts, rockets and internal combustion engines, both at design and off-design points. Greater discussion of the model can be found in its documentation and publications over the years [23, 39].

The analyses in this thesis used a separate-flow turbofan, with engine components shown in Figure 3-2. At the design point, NEPP calculates engine performance through thermodynamic relations using user-specified efficiencies, pressure ratios and other cycle parameters. At the off-design conditions, NEPP employs scalable component maps to perform component matching and satisfy continuity of mass, momentum and energy.

The engine cycle design variables in Caffe include sea-level static (SLS) thrust, overall pressure ratio (OPR), bypass ratio (BPR) and combustor exit temperature (T_{t4}). Inlet mass flow and fuel flow rate are adjusted in NEPP to ensure that these

parameters are met at the design point of SLS conditions. The engine is run at a suite of conditions for the purposes of mission analysis in Caffe, each of which has its own throttle position, Mach number and altitude. This includes takeoff, climb, cruise, approach and landing conditions. The throttling at off-design conditions is handled by adjusting T_{t4} until a desired thrust setting is obtained.

3.3.2 Emissions Module

The emissions tradeoffs and investigations into EDS in this thesis focused on NO_x emitted during the landing-takeoff cycle ($LTO\text{-}NO_x$). The emissions index predicted for NO_x, EI_{NO_x}, was based on a correlation of the temperature and pressure entering the combustor within NEPP. The standard NEPP correlation is given by,

$$EI_{NO_x} = 0.004194 \left(\frac{P_3}{439} \right)^{0.37} \exp \left(\frac{T_3 - 1471}{345} \right) T_4$$

where the subscript 3 refers to combustor entrance, 4 refers to combustor exit, P is taken in psi and T is taken in $°R$. To obtain a total emissions output from an emissions index (for a single engine),

$$NO_x = \int_0^t \dot{m}_f \cdot EI_{NO_x} dt$$

where $\dot{m}_f$ is the fuel flow rate and t is the segment time.

Although the same correlation was used throughout the various mission segments, corrections should have been to the predicted EI_{NO_x} at cruise or landing conditions to account for the variable ambient atmospheric and humidity conditions. These modeling deficiencies are subjects of ongoing research and improvement in Caffe.

There are many other emissions species besides NO_x. Hydrocarbons, SO_x, soot and other emissions particulates are areas of future research and were not modeled here. However, although the investigations in this thesis did not focus on CO_2 emissions, its prediction does not require calibrated correlations or empirical data. CO_2 calculations are simply a product of fuel burn based upon equilibrium chemistry,

$$H_x C_{2x} O_x + \left(\frac{7}{4} x \right) O_2 \rightleftharpoons (2x) CO_2 + \left(\frac{x}{2} \right) H_2 O$$
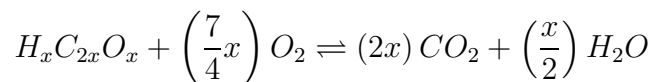
3.3.3 The Noise Prediction Module, ANOPP

The NASA Aircraft Noise Prediction Program is a well-known and widely used tool for aircraft noise prediction developed in the 1970s. At the time of its development, aircraft noise was a relatively new topic in industry and research. ANOPP's modular
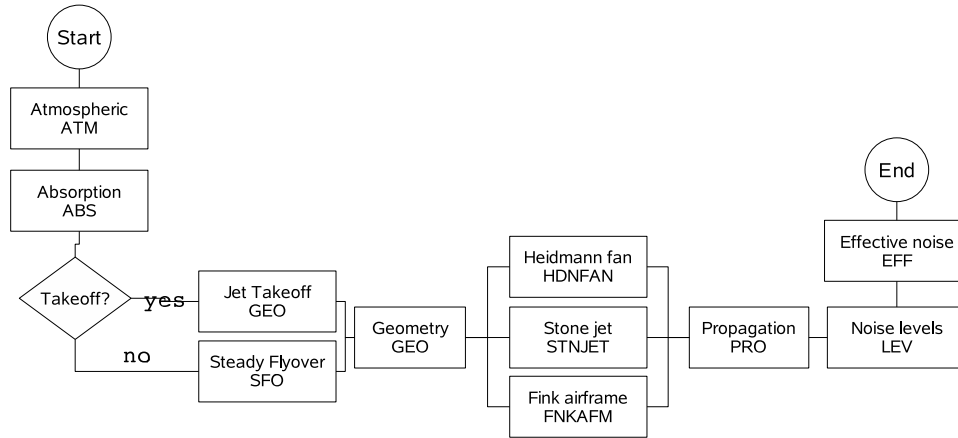
Figure 3-3: ANOPP code flow in Caffe. Adapted from [3].

structure, script-able executions and database management were at the forefront of software development in the 1970s.

Over the many years of its development, many modules have been created for ANOPP, each of which is responsible for a different aspect of aircraft noise generation and management. In Caffe, the execution structure is shown in Figure 3-3. The noise analysis methods in ANOPP differ slightly between the approach point and the two takeoff points. For takeoff, a time-dependent noise calculation is done as the aircraft accelerates from rest through its takeoff profile. During approach however, the aircraft has a relatively constant velocity so the noise calculation is assumed to be time-independent and considered a steady flyover. Nevertheless, for all FAR36 points, the same ANOPP noise modules are used:

1. Fan noise (Heidmann model)[17]

2. Jet noise (Stone model)[42, 43]

3. Airframe noise (Fink model)[12]

3.3.4 ANOPP Assessment

As it grew into a cohesive piece of software and as an engineering tool, ANOPP became subject to a handful of assessment studies over its lifetime. These studies are presented here as a literature survey of NASA technical reports and investigations.

Early ANOPP Assessment Studies

1979 McDonnell Douglas Study Of all of the assessment studies, the first was the smallest in scope and the most sparing in detail. The study consisted of a flyover

test of a DC-10-40 with two JT9D-59A engines. When comparing ANOPP results with the flyover data, the author reported that ANOPP tended to over-predict fan inlet noise up to 15 PNL in the forward arc and over-predict fan exhaust noise in the aft arc while under-predicting jet and core noise at low frequencies. Few other comments or recommendations were made [20].

1980 Boeing Study The Boeing study in 1980 was more thorough than the Mc-Donnell Douglas study the year previous. Boeing also performed a flyover test, but used a 747-100 with three JT9D-3A engines and one JT9D-7CN engine. The study involved multiple flyovers at different throttle settings [40].

In comparison with ANOPP predictions, Boeing concluded that ANOPP under-predicted low frequency noise levels for all angles and power settings from 5–15dB, where the jet noise model was the primary culprit for the discrepancy. In the middle and high frequency range, ANOPP over-predicted noise levels by about 10dB in the forward arc for high power settings and around 2-6dB on approach throttle settings. The fan inlet noise model, specifically the buzzsaw or tone module, was the chief contributor to the error.

A detailed analysis of the ANOPP modules exposed specific shortcomings. The jet noise model suffered from under-prediction of 2-15dB. The fan buzzsaw model over-predicted takeoff noise in the forward arc by 10-15dB, but under-predicted approach noise by 10-20dB. Finally, the turbine noise model under-predicted noise at takeoff at angles of $120°$–$150°$ by 15-20dB and 5-7dB at approach.

Recent ANOPP Assessment Studies

1996 GEAE Study Unlike the previous two investigations, the 1996 GEAE study focused on noise arising from the engine exclusively. GEAE sought to quantify and understand ANOPP's reputation for over-prediction of noise. They compared ANOPP predictions to noise data for the the CF6-80C2, Energy Efficient Engine (E^3), Quiet Clean Short Haul Experimental Engine (QCSEE) and the CFM56. ANOPP was also compared to GE noise models [24].

The GEAE analysis examined the ANOPP modules one by one. The fan inlet noise model (Heidmann model) was found to be the most significant contributor to over-prediction by ANOPP. It suffered from over-prediction at all power settings, takeoff through approach, in the forward arc and was quite sensitive to relative fan tip Mach number (M_{Tr}). For subsonic M_{Tr} numbers, ANOPP under-predicted noise by 0.5–5db and for supersonic M_{Tr}, ANOPP over-predicted noise by 11-19dB.

The conclusions made for the other ANOPP modules were less severe than the assessment of the fan inlet noise model. The fan exhaust noise model over-predicted noise for the E^3, but under-predicted for the QCSEE. For the CF6, the fan exhaust

model over-predicted at takeoff, but under-predicted for cutback and approach throttle settings. The jet noise model also had a tendency to over-predict noise by 1-6dB, especially at lower velocities for the CF6 and the QCSEE. The combustion noise model in ANOPP demonstrated good agreement with the GE model. Finally, the turbine noise model in ANOPP predicted noise levels up to 30dB higher than the GE model.

In contrast to the previous ANOPP assessments, the GEAE report made specific recommendations for improvement. Specifically, GEAE suggested changes in the fan noise inlet model, which have since been implemented as an option in ANOPP. Thus, ANOPP has become much more accurate in overall noise prediction since the GEAE study in 1996.

Small Engine Technology Tasks   At the same time of the GEAE study, Allied Signal and Honeywell began to validate ANOPP for small turbofan jet engines. Both companies produced engines for the regional jet market and worked with NASA to expand ANOPP's capabilities. The semi-empirical databases for fan noise, combustion, turbine and jet noise were updated with smaller engine data [18]. A wing-shielding and reflection module was also incorporated into ANOPP since regional jets often support their engines on the fuselage above and behind the wings [27]. These efforts augmented the accuracy of ANOPP for regional aircraft and small turbofans in general. Since all of the studies in this thesis revolved around large, commercial aircraft and engines, these improvement efforts were not seen.

ANOPP Assessment Conclusions

None of the above assessments concluded with complete approbation of ANOPP's predictive capabilities. ANOPP is semi-empirical, so it attempts to correct theoretical shortcomings with experimental data. Unfortunately, noise measurements and full-scale aircraft or engine noise tests require an expensive testing infrastructure. Many of these test locations belong to industry, who are loathe to disclose their proprietary test results. Thus, building a database of versatile noise data that could be applied to many different types of aircraft and engines remains an incomplete task.

Despite its incomplete empirical databases, ANOPP has improved over the course of its development. The above assessment studies and NASA development have focused on the engine fan, jet and airframe modules, as those tend to dominate the aircraft noise signatures. The other modules for combustion, turbine and acoustic liners have so far eluded rigorous assessment. Therefore, the noise studies in this thesis only included fan, jet and airframe noise sources because it was felt that the other modules were too poorly calibrated. Moreover, ANOPP noise predictions for the three FAR 36 certification points were never compared to actual data because it was already known

Table 3.2: Input design variables and applicable constraints for integrated framework case study.

Design Variables	Constraints
Engine	6000 nm cruise range
BPR, OPR, T_{t4}, SLS Thrust	9000 ft takeoff field length
Mission	8000 ft landing field length
Initial, final cruise altitudes	Twin engine
Wing Geometry	200 ft span limit
S_{ref}, AR, t/c, sweep, x-location	Stability constraints
Horizontal tail area	Drag constraints

that ANOPP fails to accurately predict real aircraft noise performance. Depending on the frequency and directivity angle, the above validation studies suggest that ANOPP results can over or under-predict experimental data by as much as 5–10 dB. Nevertheless, as a semi-emprical code with grounding in acoustic theory, ANOPP is still trend accurate and its results can easily be compared against a baseline analysis. The studies in this thesis that focused on noise metrics always compared two ANOPP results together. ANOPP predictions were never evaluated against actual data.

3.4 Integrated Framework Case Study

A design optimization case study was performed to convey the drawbacks of an engine-focused analysis of the environmental design space compared to an integrated aircraft-engine approach. One might postulate that since noise and emissions are engine-focused phenomenon, the design tool should be engine-focused as well. The case study optimization centers around a 275 passenger aircraft flying a cruise range mission of 6000 nm. Aircraft designers often seek to reduce GTOW as much as possible as a surrogate for cost. Similarly, this optimization adjusted high-level design variables to minimize GTOW. The design variables used included engine parameters, aircraft geometry and cruise altitudes. All of the design variables and constraints used in the case study are listed in Table 3.2.

3.4.1 Procedure

To give the case study a baseline aircraft and starting point for other computations, the aircraft was initially optimized for minimum GTOW using all of the design variables. This initial optimization closed the design, meaning the optimizer found a location in the design space that satisfied all of the applied constraints. From the baseline, closed design all other optimizations were launched. These additional analyses began

Table 3.3: Parametric sweep of current and future technology levels for BPR, FPR and OPR.

		OPR					
BPR	FPR	35	37	39	41	43	45
3.9	1.8						
5.3	1.7						
6.89	1.6						
8.81	1.5						
11.3	1.4						
15.5	1.3						

with a parametric variation of OPR and BPR. The OPR and BPR were held constant at a test matrix of values that swept current and future technology levels, as listed in Table 3.3. For a given BPR, the methodology used to select the engine cycle uniquely determined a fan pressure ratio (FPR). While this was a byproduct of the computational approach, it is generally true that for a given OPR and BPR there is an optimal FPR. Thus, as BPR and OPR were held constant, so too was FPR fixed at each point.

At each combination of OPR and BPR, two different re-optimizations for GTOW were performed with different design variables. In the first set of re-optimizations, the optimizer only had access to the remaining engine design variables (SLS Thrust and T_{t4}), while in the second set the optimizer was given access to all of the remaining design variables (aircraft and engine). Thus, the first set of re-optimizations focused on the engine entirely, while the aircraft geometry remained fixed. The second set of re-optimizations allowed for the redesign of both the engine cycle and the aircraft as the BPR and OPR varied.

3.4.2 Results and Discussion

The results of the two sets of re-optimizations were compared within a section of the environmental design space. The re-optimizations were plotted in terms of GTOW and $LTO\text{-}NO_x$. Each set, therefore, constructed a carpet plot with vertices at the various BPR and OPR values.

The engine-only optimization is shown in Figure 3-4a. Lines of constant BPR travel along the x-axis while lines of constant OPR travel along the y-axis. As expected, the higher the OPR, the higher the $LTO\text{-}NO_x$ since the temperature of combustion increases with pressure ratio. However, the GTOW of the aircraft remains more or less constant, indicative of the fact that the optimizer only had access to the engine cycle parameters while the aircraft geometry remained fixed. The GTOW is essentially constant at its baseline value, with the small changes reflecting variable engine weight

Table 3.4: Detailed comparison of engine-only and aircraft-and-engine re-optimizations for $FPR = 1.7$ and $OPR = 35$ ($BPR = 5.3$)
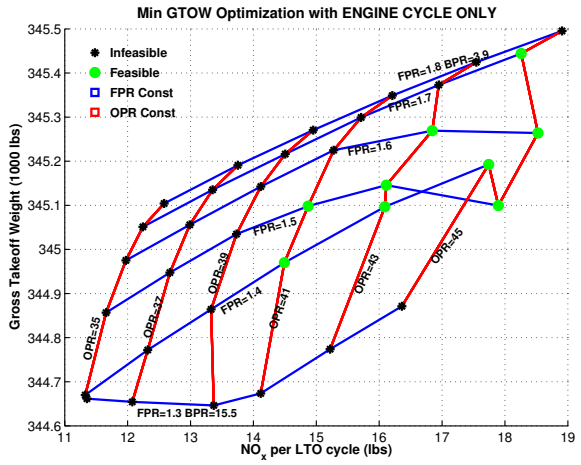
Variable	Engine-only	Aircraft & engine
S_{ref} (ft^2)	$3,317$	$3,326$
AR	7.91	7.43
t/c (%)	12.54	12.96
T_{t4} (°R)	$2,847$	$2,887$
SLS Thrust (lbs)	$58,376$	$64,252$
Cruise range (mi)	$5,562$	$6,009$
Fuel weight (lbs)	$121,372$	$136,733$
GTOW (lbs)	$345,051$	$360,377$

and fuel weight.

It is important to note that the points in Figure 3-4a are marked either *feasible* or *infeasible*. An optimization is considered feasible if it meets all of the applied constraints. Most of the points in Figure 3-4a are in fact infeasible because they fail to meet the cruise range requirement of 6000 nm. The optimizer did not have enough degrees of freedom to arrive at a valid design. This is a key shortcoming in engine-focused analysis. Ignoring the aircraft in design tradeoff studies might often lead to plausible, yet erroneous results.

The set of re-optimizations for the aircraft *and* engine design variables, shown in Figure 3-4b, offers a significant contrast to the engine-only set. The tail of the carpet plot, corresponding to high BPR, wraps upward towards higher GTOW. This is because for the thrust class of the engine, a BPR around 15 overpowers the cycle and creates a large fan face which compounds nacelle drag so performance degrades. Moreover, the larger fan diameter leads to a much heavier engine that the aircraft must support. Also, unlike the engine-only optimizations, all points in the aircraft-and-engine set are feasible designs.

The two carpet plots are displayed on the same set of axes in Figure 3-4c. The entire engine-only set of re-optimizations collapses to appear as one thick line next to the aircraft-and-engine optimizations. This is again attributable to the small variation in GTOW in the engine-only set. A point comparison is made to gain greater insight into the reason that a point in the engine-only set was infeasible yet feasible in the aircraft-and-engine study. The point of interest is for a $FPR = 1.7$ and $OPR = 35$ ($BPR = 5.3$), with the optimized design variables detailed in Table 3.4. These design variables give physical insight into the problem. The engine-only re-optimization fell short in the cruise range requirement by nearly 500 nm. To overcome this shortfall, the aircraft-and-engine re-optimization was able to resize the wing to hold more fuel and meet its range requirement. Without the aircraft variables in the design space, a feasible design was unattainable.

(a) Engine only
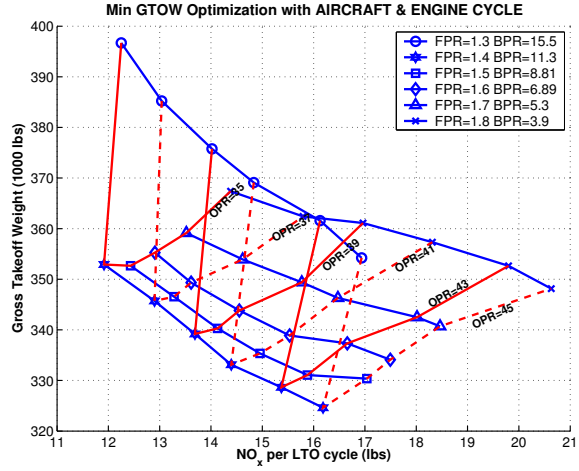
(b) Aircraft & engine
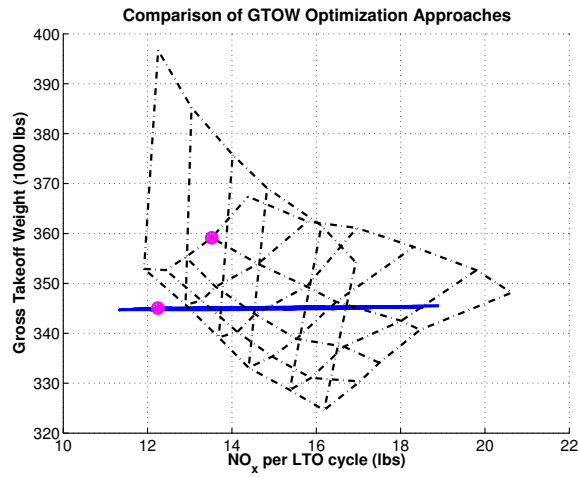
(c) Comparison with point emphasis at
$FPR = 1.7$ and $OPR = 35$ $(BPR = 5.3)$

Figure 3-4: Case study results for GTOW minimization.

3.5 Summary

This chapter gave a detailed description of the EDS framework design tool, Caffe and its various modules. These modules include those part of the Stanford PASS system and two NASA codes. The environmental metrics of $LTO\text{-}NO_x$ and cumulative EPNL are generated by these NASA codes. Emissions prediction is a correlation in NEPP based on T_3, P_3 and T_4 and noise prediction is handled by ANOPP utilizing its fan, jet and airframe noise modules. It is generally accepted that ANOPP is not successful in capturing actual aircraft noise performance, but can be used for relative comparisons since it is trend accurate. To demonstrate Caffe functionality and capability, an example case study was presented that adduced the use of an integrated aircraft-engine design tool and delineated the pitfalls of engine-only thinking.

Chapter 4

Model Assessment

4.1 Introduction

Assessing the validity, accuracy or level of uncertainty of a model is a concept that arises often in engineering [16]. While the understanding of the realm of applicability or level of fidelity of an analysis tool is addressed in the literature (as reviewed in Section 1.3), there is no universally accepted algorithm by which to proceed. Thus, this chapter begins by devising and discussing the elements of a *probabilistic model assessment methodology*, which is preferred to account for the inherent uncertainty in validation studies.

The methodology for assessment, once described, is applied to the engine cycle deck module of Caffe, NEPP. This is executed by comparing NEPP estimates of performance for example engines to publicly available data. The assessment of NEPP is both a demonstration of the probabilistic methodology and an inroad into the larger task of comprehensive assessment of the EDS framework.

4.2 Probabilistic Assessment Methodology

This section presents a general, probabilistic assessment methodology that is later applied to NEPP. This approach is most similar to that of Baghdasaryan et al. [6], who present a probabilistic model validation scheme that uses Monte Carlo simulations of meta-models, such as RSMs, to express the uncertain response of models as a PDF. The model output is compared to experimental data, which thereby discerns both the *modeling error* and *modeling uncertainty*. For Baghdasaryan et al., a model is accepted if the confidence interval of the experimental result is within a user-specified tolerance. Baghdasaryan et al. also emphasize the importance of validation at multiple design points, in which case multiple PDFs are combined into joint probability distributions, and demonstrates this technique on a finite-element model of sheet metal flanging.

Compared to [6], the procedure developed in this thesis is a similar conceptualization of uncertain model outputs and assessment at multiple design points, as described in Section 4.2.3, but goes further to address the sensitivities of the user decisions. Baghdasaryan et al. do not quantify the impact of the user upon the validation results. Furthermore, whereas Baghdasaryan et al. arbitrarily penalize the variability of the outputs to account for experimental and RSM error, a Monte Carlo simulation of the direct model is maintained here. The procedure developed is the following,

1. Selection of probabilistic inputs

2. Selection of distributions for the inputs

3. Monte Carlo simulation of all the inputs

4. Sensitivity studies

    (a) Key drivers of uncertainty
    (b) Dependence of outputs on input distribution parameter selection

5. Propagation of module uncertainty to system level

4.2.1 Selection of Probabilistic Inputs

Many analytical or design modules require numerous inputs. Employing every input and parameter in an assessment study, especially a probabilistic study, would be too computationally intensive. Instead, the user must select the most uncertain or most influential variables for further investigation. While the list of inputs might be long, not all would be key drivers of the output metric of interest. For higher fidelity models, where the number of inputs is quite large, a more systematic approach might be employed. All of the inputs could be classified as one of the following,

Important The variable is estimated to be a key driver of the output metric of interest.

Necessary The variable must be specified in order to run the model, but is not necessarily a key driver of the output.

Ignore The variable is not a key driver of the output metric and is not required to execute the model.

Finally, all of the *important* inputs could be further categorized as either known or unknown. The unknown inputs are those that should be used in the Monte Carlo simulations.

4.2.2 Selection of Distributions for the Inputs

Once the stochastic inputs are selected, they require probability distributions. Engineering judgment, experience or even empirical evidence might guide the decision, but there is no closed form method by which input distributions can be chosen. Both the shape of the distribution and the parameters for that shape must be selected. Model assessment often involves uncertainty in knowledge about the inputs. This uncertainty can be assumed to be normally distributed (Gaussian distribution) about a mean value. However, engineering experience or empirical evidence might suggest a more sophisticated distribution. Moreover, thinking in terms of *confidence intervals* enables quick selection of both means and standard deviations for normal distributions. For instance, instead of trying to think of a mean and standard deviation for parameter X, try to think of being able to state, with 95% confidence, that parameter X will assume values between a and b. The average of a and b is then the mean value and one-fourth of the difference is the standard deviation. Due to the subjective nature of the input parameter selection process, sensitivity studies are performed to characterize the level of influence the selection has upon the output metrics.

4.2.3 Monte Carlo Simulation of Probabilistic Inputs

A Monte Carlo simulation constructs the output metric of interest from the input probability distributions. If this output metric is compared to an accepted standard, perhaps published or experimental data, then the output distribution from the simulation becomes a distribution for percent error, such as Figure 4-1. Each case in the computation would generate one discrete point, with some percentage error, and thousands of points would create a histogram. The uncertainty and variability of the input parameters leads to uncertainty of the output as well. Since the inputs cannot be known perfectly, the output cannot be known perfectly either. The *modeling uncertainty* would thereby be an artifact of the input uncertainty. Modeling uncertainty refers to the spread of plausible, legitimate outputs the model might generate. In addition to the modeling uncertainty, a Monte Carlo simulation allows the *modeling error* to be assessed as well. The zero percent error run, where the model exactly predicts the published performance data, would occur at some confidence interval. If that confidence interval is within some user specified tolerance, perhaps 95%, or 2σ, then the modeling error would be less than the scope of the modeling uncertainty. Therefore, the conclusion would be that the error inherent in the model is subsumed within the scope of modeling uncertainty. However, if the modeling error were beyond the confidence interval, then the error in the model would be greater than the input uncertainty. In that case, the user must evaluate whether the level of modeling error is acceptable or not.
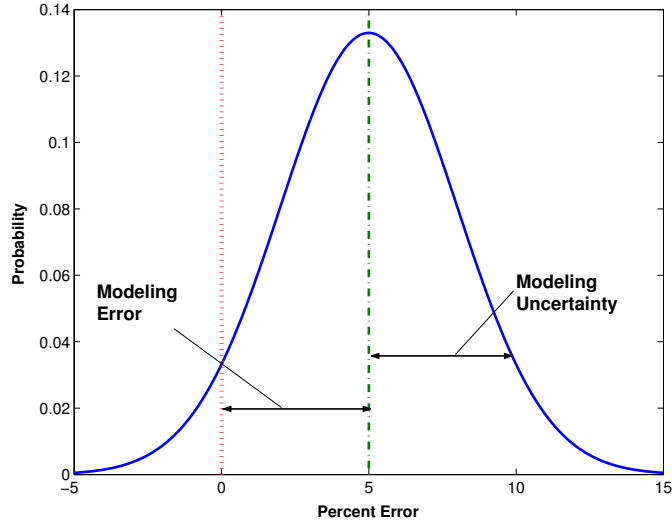
Figure 4-1: Sample output from Monte Carlo simulation of uncertain inputs

4.2.4 Sensitivity Studies

Although the initial Monte Carlo simulation and outputs such as Figure 4-1 address error and uncertainty, further interrogation of the model and input distributions is required. Numerous input uncertainties coalesce to generate Figure 4-1 and those input distributions themselves were selected subjectively. The impact of each individual input and the sensitivity of the output to the choice of distribution must be characterized.

Identifying the input variables with the largest influence upon the output uncertainty is done through additional Monte Carlo simulations. If one of the probabilistic variables were held fixed at its nominal value and the remainder of the inputs were used in a Monte Carlo simulation, the output distribution would most likely change. The change in mean and variance of the output from the initial simulation to the one where a specific input was held constant would identify the severity of impact for that input. This approach is called *let-all-but-one-vary* Monte Carlo simulations to flag the key drivers of uncertainty. This is preferred over *hold-all-but-one-constant*, so that most of the interactions between parameters, if any, are preserved. While computationally expensive, let-all-but-one-vary is the appropriate technique when dealing with complex design tools. The importance of capturing interactions between variables, especially when allocating sensitivities, cannot be over-stated. It is almost certain that the inputs to a complex design tool are correlated at some level. Other sensitivity analysis methods, such as finite difference gradients and multi-variate regression, have difficulty in capturing these correlations, whereas they are automatically included in
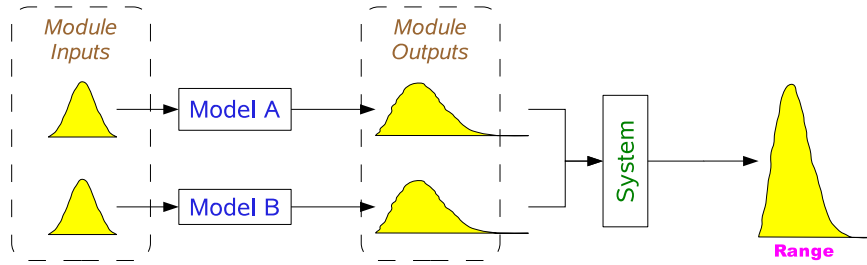
Figure 4-2: Propagation of uncertainty from the module level to the system level

the let-all-but-one-vary approach.

The sensitivity of the Monte Carlo results to the selection of input distribution parameters can be done by scaling or perturbing the distributions. If the standard deviations of normal distributions were doubled or halved and then used in another Monte Carlo simulation, one could observe if the modeling error remains contained within the modeling uncertainty. The same approach could be used for the mean values of a normal distribution by shifting them slightly from their initial values.

4.2.5   Propagation of Module Uncertainty to System Level

Tracking the uncertainty of module inputs to the output level is only one layer of probabilistic assessment. Complex analysis or design tools are comprised of numerous modules interacting and exchanging information. Each of these modules have inputs, and therefore output uncertainties, of their own. Understanding how the input uncertainty of a specific module propagates to the system level outputs is also important. The uncertainty of one module might either amplify or negate the uncertainty of another. This can only be determined by propagating and compounding the uncertainty one module at a time, as in Figure 4-2.

4.3   NEPP Assessment

The probabilistic assessment methodology was applied to Caffe's engine cycle deck. While NEPP is a versatile and extensive tool capable of capturing many types of propulsion systems, this study focused on the model assessment for commercial turbofans at takeoff and cruise conditions. The output metrics of interest were takeoff and cruise thrust specific fuel consumption (TSFC), as they address performance of the entire engine at key flight conditions.

The NEPP assessment study used the CFM56-5A1, the General Electric GE90-90B and the Pratt & Whitney PW4056 as example engines for analysis. These three

Table 4.1: Baseline engine specifications and performance [14, 19].

Variable	CFM56-5A1	GE90-90B	PW4056
BPR	6.00	8.36	4.70
OPR	26.60	39.38	29.30
TO Mass flow [lb/s]	852	3,195	1,705
TO Fuel flow rate [lb/h]	8,333	26,572	19,445
TO thrust [lbs]	25,000	94,000	56,750
TO TSFC [lb/h/lb]	0.333	0.283	0.343
Certification date	8/87	4/95	1/85

engines span the previous 20 years of technology and offer a range of bypass ratios, thrust classes and technology. Some published data and parameters of these engines are available, as seen in Table 4.1.

4.3.1 NEPP Probabilistic Inputs and Distributions

The NEPP documentation and input files were canvassed to compile the catalog of inputs and outputs. Variables were given either the classification of *Important*, *Necessary* or *Ignore*, as described above. The input variables were given their classification based on estimation whether or not those variables would be strongly correlated with the outputs. Consideration was also given to the variables that might be the focus of new technologies for improvement in the next 20 years. The *important* inputs were further refined and classified as either known or unknown. Finally, the unknown inputs were given probability distributions, as detailed in Table 4.2. Although the sensitivity of the distribution selection is discussed below, the sensitivity of including or not including a particular variable is not addressed.

All of the input distributions were considered to be Gaussian, with special consideration given for the FPR. While the FPR was just as uncertain as the other inputs, it was also known that FPR scales inversely with BPR. Thus, the FPR for the GE90 with a BPR of 8.4 would be smaller than the FPR for the PW4056 with a BPR of 4.7. Therefore, a customized FPR distribution was given to each engine to reflect this relationship with BPR.

For the normally distributed inputs, the mean values were estimated by examining example engines from other engine cycle deck programs, such as GasTurb and GECAT (an educational, GUI-based version of NEPP). These values were corroborated with proprietary engine data from Pratt & Whitney. The standard deviations were estimated by considering confidence intervals for a parameter. For instance, it was estimated that the 95% confidence interval for fan adiabatic efficiency lies between 0.85 and 0.93. From that estimate, the mean fan efficiency would be 0.89 and the 2σ

Table 4.2: Normally distributed variables for `NEPP` assessment Monte Carlo simulation.

Variable	Encoding	Mean	2σ
Fan operating point	`rc1`	1.32	0.5
LPC operating point	`rc2`	2.00	0.5
HPC operating point	`rc3`	2.00	0.5
Fan pressure ratio	`pic1`		
CFM56-5A1		1.65	0.05
GE90-90B		1.55	0.05
PW4056		1.70	0.05
LPC pressure ratio	`pic2`	1.50	0.4
Fan efficiency	`etac1`	0.89	0.04
LPC efficiency	`etac2`	0.90	0.04
HPC efficiency	`etac3`	0.865	0.04
% bleed flow after LPC	`mbldc1`	0.055	0.04
% bleed flow after HPC	`mbldc2`	0.18	0.04
HPT operating point	`rt1`	4.80	0.7
LPT operating point	`rt2`	5.50	0.5
HPT efficiency	`etat1`	0.92	0.04
LPT efficiency	`etat2`	0.93	0.04
% bleed flow into HPT	`mbldt1`	1.00	0.2
% bleed flow into LPT	`mbldt2`	0.30	0.2
% HPT bleed into HPT inlet	`mbldint1`	0.65	0.2
% LPT bleed into LPT inlet	`mbldint2`	0.55	0.2
Cruise throttle setting	`crth`	0.85	0.05
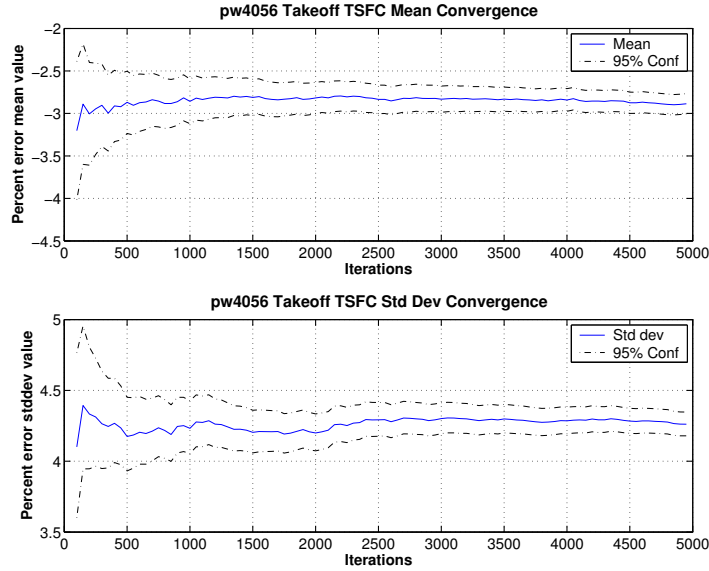
Figure 4-3: Convergence histories of the Monte Carlo population mean (top) and standard deviation (bottom) for the 95% confidence band.

value would be 0.04. The sensitivity of the end results to these assumptions will be addressed later in this chapter.

4.3.2 Monte Carlo Simulation Execution

Monte Carlo simulations of the three engines at both takeoff and cruise conditions were executed. The estimated TSFCs for these two flight conditions were compared against actual performance data. Table 4.1 includes the takeoff TSFCs for the engines from publicly available data. The only cruise TSFC data obtained was for the GE90-90B from proprietary sources. Therefore, the GE90 is the only engine for which assessment studies at cruise are presented. Despite its computational costs, a full Monte Carlo analysis was preferred over a meta-model, such as RSM, to capture the complexities of aerodynamic systems [13, 45].

The normally distributed input distributions listed in Table 4.2 were randomly sampled 5000 times in a Monte Carlo iteration. To verify that 5000 was a sufficient iteration number, the 95% confidence interval for the population mean and standard deviation were plotted, as shown in Figure 4-3. The confidence band after 5000 iterations was considered acceptable for convergence. The details of Monte Carlo simulation convergence were discussed in Section 2.3.3.

On-Design Takeoff Results

The resulting distributions for takeoff TSFC for the three engines are shown in Figure 4-4 with the solid red line indicating the 95% confidence interval. The zero-percent error mark, where NEPP exactly predicted reported engine performance, falls within the confidence interval for all three engines. For the GE90 and CFM56, the zero-percent error mark was only marginally contained in the confidence interval, whereas for the PW4056 the zero-percent error mark is more centered in the confidence interval. This phenomenon will be discussed and analyzed at length in Section 4.3.5. The distributions also show significant variability. While the zero-percent error mark is within the 95% confidence interval, that interval spans from -15.3% to 0.7% for the CFM56. This degree of variability has implications for all system-level analyses and is further scrutinized in Section 4.3.3.

Off-Design Cruise Results

At the on-design condition, NEPP uses the user specified pressure ratios and efficiencies to solve standard thermodynamic relations to obtain engine performance. At the off-design points, however, NEPP employs scalable component maps and solves a series of equations to satisfy matching requirements. Thus, many more variables come into play at the off-design case and should be treated separately from the on-design assessment results.

As mentioned above, cruise TSFC performance data was only available for the GE90-90B. The output distribution is shown in Figure 4-5. In contrast to the on-design takeoff condition where the zero-percent error mark was just contained within the 95% confidence interval, the zero-percent error mark at cruise is more centered within the confidence interval. This suggests that errors that perhaps pulled NEPP in one direction at the takeoff condition were negated by either new errors that arose at the cruise condition or the inclusion of the off-design component maps variables.

4.3.3 NEPP Sensitivity Analyses

In a probabilistic analysis, there are many steps that involve engineering decisions. The selection of stochastic inputs and the distributions for those inputs are the most common. A sensitivity analysis aimed to quantify the level of impact of these choices upon the NEPP assessment results.

Key Drivers of Uncertainty

At the outset, it was not known which variables would be the most influential upon the output metric of interest. The selected probabilistic inputs and their distributions
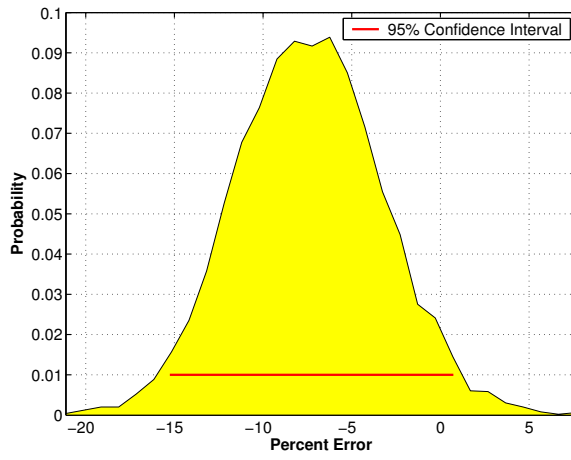
(a) CFM56-5A1
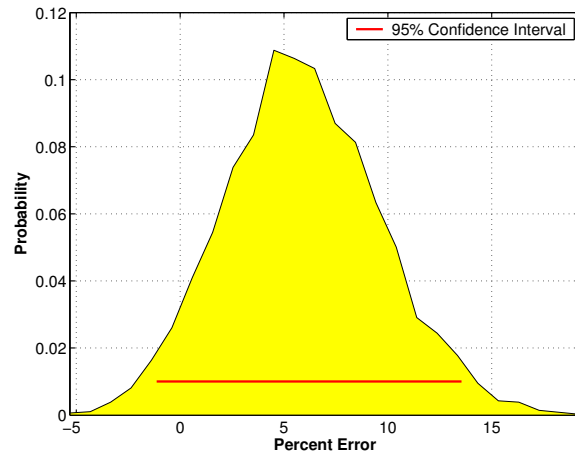
(b) GE90-90B
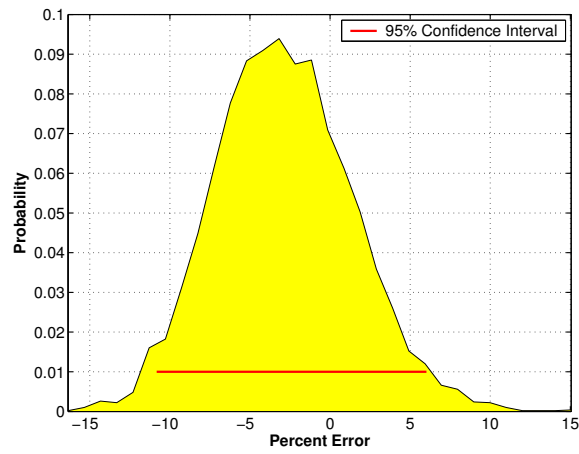
(c) PW4056

Figure 4-4: Takeoff TSFC distribution as percent error from published data.
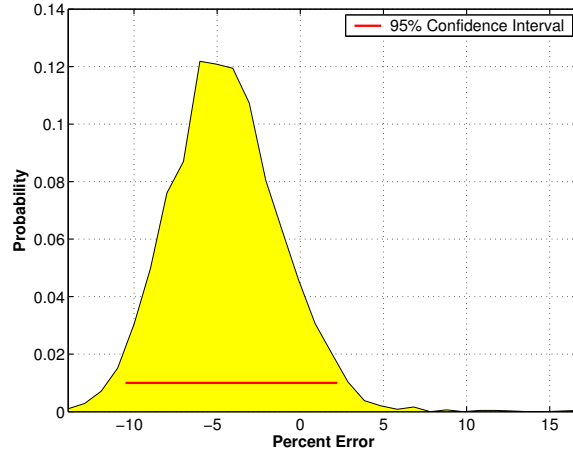
Figure 4-5: Cruise TSFC distribution as percent error from actual data for the GE90-90B.

in Table 4.2 are the byproduct of engineering decisions. To quantify their levels of impact, a *let-all-but-one-vary* series of Monte Carlo simulations was performed for each input, as described above in Section 4.2.4. Figure 4-6 depicts a comparative bar chart for the change in variance of the resultant takeoff TSFC distribution when each variable is held constant. The key drivers of uncertainty are the fan and HPC adiabatic efficiencies, the turbine adiabatic efficiencies, and the amount of bleed flow into the HPT.

The off-design cruise condition involves many more variables and was treated separately in the sensitivity analysis as well. The comparison of changes in uncertainty for the GE90 at cruise is shown in Figure 4-7. The contributions to overall variance of the key drivers in the takeoff condition are smaller at the cruise condition. The variability of the operating point on the fan component map also appears as one of the key drivers.

Figures 4-6 & 4-7 identify the variables that contribute most to the output variance. However, it is quite likely that information about some of the key drivers will be more available than others. Meaning, obtaining information on pressure ratios would most likely be easier than accurately predicting the LPC operating point in the off-design case. The availability of a variable's data does not necessarily correlate with its importance. For instance, although the bleed flow into the HPT was shown to be a key driver of output uncertainty, ascertaining specific bleed mass flow values might be more difficult than obtaining combustor exit temperature data. Thus, one can also think of a prioritized list of information to have in order to accurately predict the output. In this light, all of the input variables in Table 4.2 were assigned to one of the four following classifications,
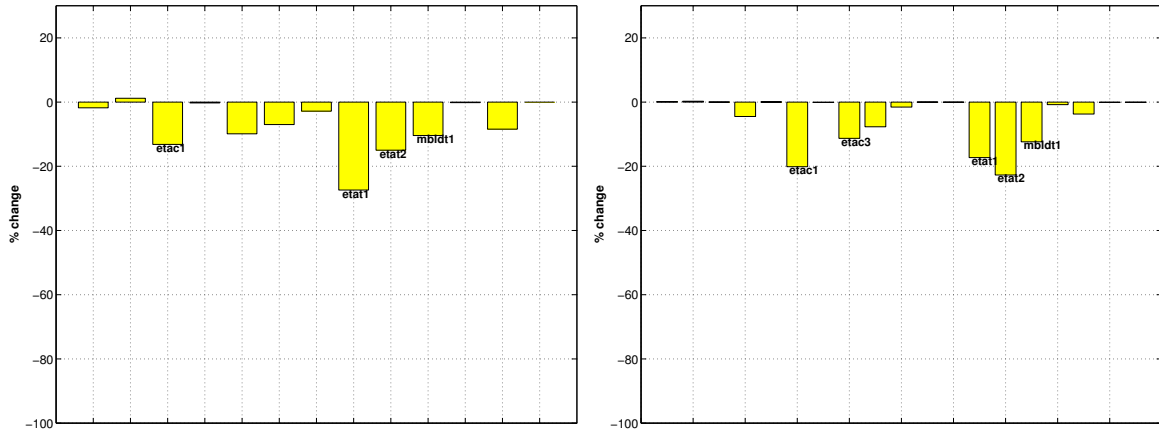
(a) CFM56-5A1

(b) GE90-90B
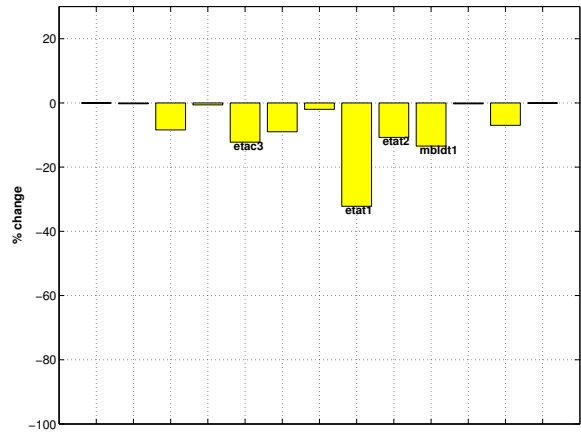
(c) PW4056

Figure 4-6: Key drivers of uncertainty through *let-all-but-one-vary* Monte Carlo simulations. Bars indicate percent change in takeoff TSFC error variance when the variable is held constant. Variables with largest impact are labeled.
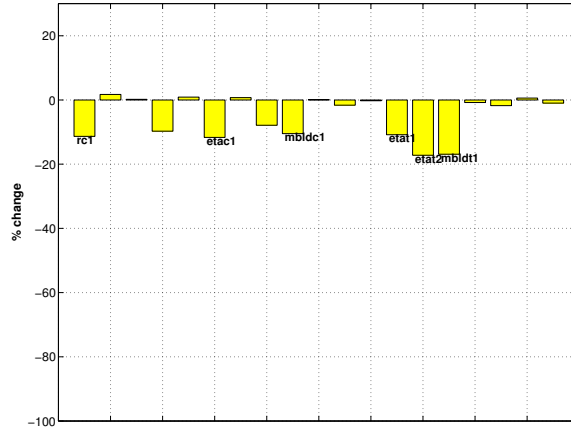
Figure 4-7: Key drivers of uncertainty through *let-all-but-one-vary* Monte Carlo simulations for the GE90-90B. Bars indicate percent change in cruise TSFC error variance when the variable is held constant. Variables with largest impact are labeled.

- Pressure ratios

- Adiabatic efficiencies

- Secondary (bleed) flow parameters

- Component map variables

These four sets of variables were independently held constant in four more *let-all-but-one-vary* Monte Carlo simulations. The comparative levels of uncertainty reduction, at both takeoff and cruise, are shown in Figure 4-8. The efficiencies are clearly the most important category of information to know at both flight conditions, with the bleed flow information second. This prioritization should be kept in mind when modeling new engines and engine technologies within EDS.

Selection of Input Distributions

Traditional sensitivity studies are comparisons of the level of influence of one variable compared to another. In a probabilistic analysis studies should also be performed regarding the selection of input distributions. It is possible that the results and conclusions would change if different means and standard deviations had been assigned to the inputs. Therefore, the sensitivity of the outputs to the selection of distribution parameters must be characterized.

The means and standard deviations in Table 4.2 were estimated by considering 95% confidence intervals. These were only estimates, so sensitivity studies of these

(a) GE90-90B Takeoff

(b) GE90-90B Cruise
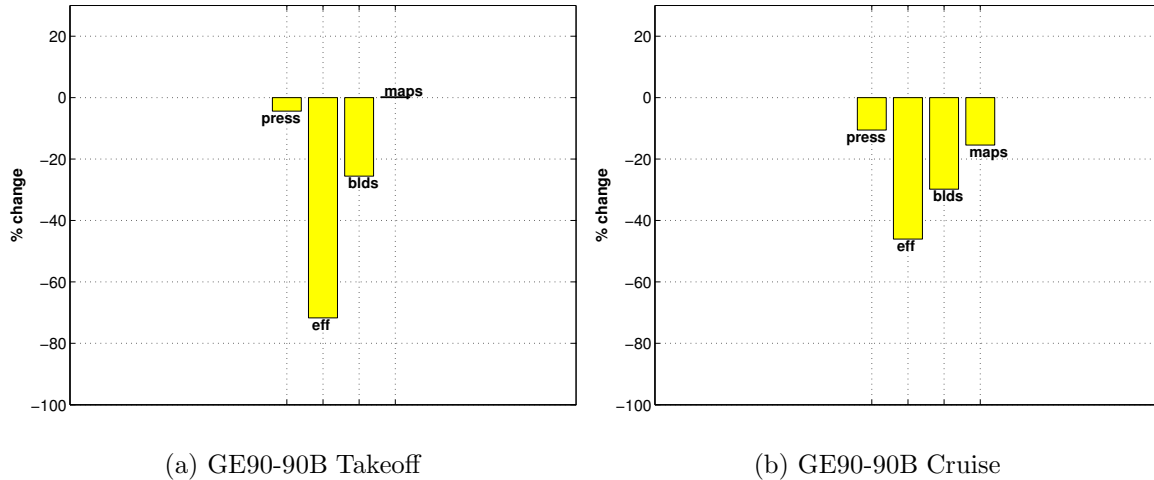
Figure 4-8: Key drivers of uncertainty when variables are classified into sets of information. Bars indicate percent change in TSFC error variance when the set of variables is held constant.

Table 4.3: Output statistics from Monte Carlo sensitivity simulations.

	Baseline	$0.99 \times \mu$	$0.5 \times \sigma$	$2 \times \sigma$
Population mean	6.3916	9.203	4.8881	9.004
Population std dev	4.1604	4.192	2.0495	13.652

parameters were executed with three additional Monte Carlo simulations of the GE90 at takeoff conditions. These three simulations involved independent perturbations to the input means or standard deviations with comparisons to the baseline distribution from Figure 4-4. The first Monte Carlo simulation involved reducing every input mean by 1% and the last two simulations involved the extreme scenarios of halving and then doubling the standard deviations. The resulting distributions are shown in Figure 4-9 with the output population statistics compared in Table 4.3.

The selection of the distribution mean is a user decision that should be made with care. Table 4.3 indicates that when the input distributions were perturbed by only 1%, the output mean shifted by 3%. On one hand, this result substantiates the use of a probabilistic approach to model assessment instead of a deterministic approach. Only considering a single value for each input can easily bias the output. However, since the 95% confidence interval in Figure 4-9b no longer contains the zero-percent error mark, it also signals that the choice of mean value has a significant bearing on the output. Figures 4-9c & 4-9d show the extreme scenarios when all of the standard
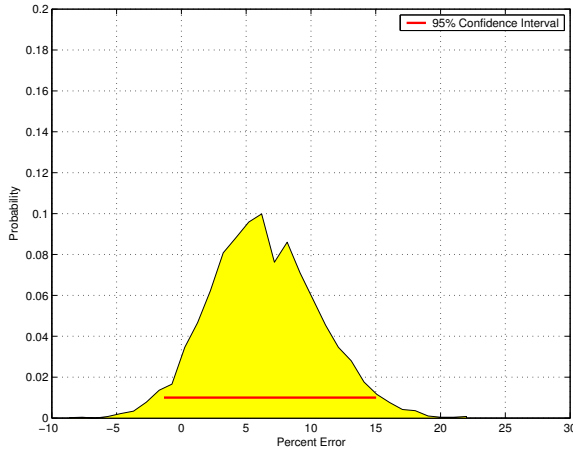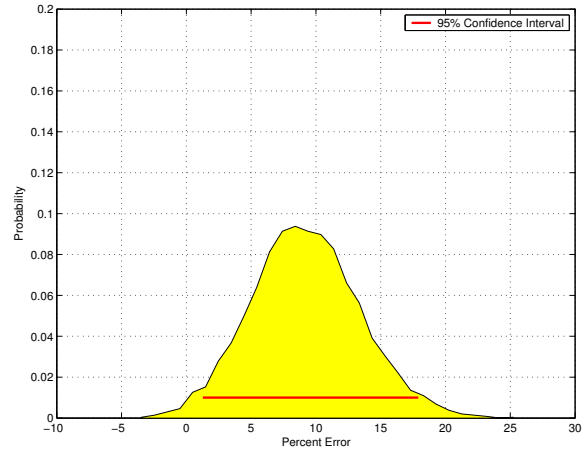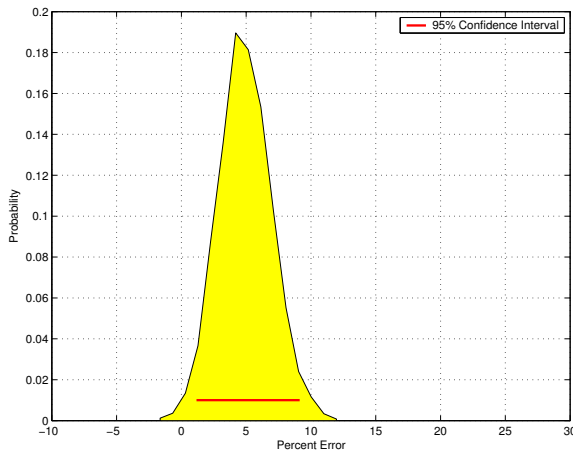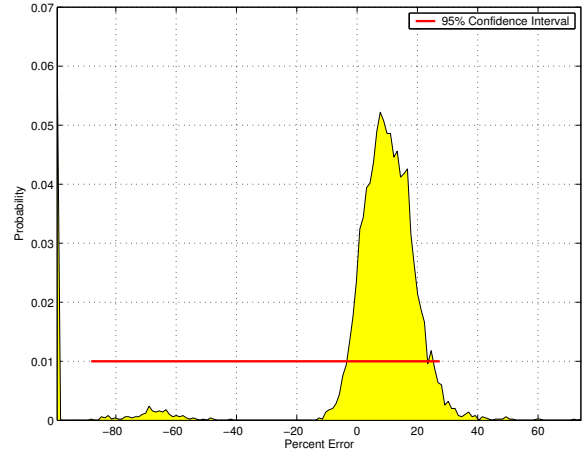
Figure 4-9: Sensitivity of output to input distributions. Baseline GE90 takeoff TSFC distribution is compared to a 1% reduction in input means as well as halving and doubling all input standard deviations.

deviations for every variable were halved and then doubled. The general shape of the distributions remains the same in both cases, although the distribution for the doubling of the standard deviations includes some iterations where the combination of input values created extreme, perhaps numerical, errors. As above, it is important to note that when the standard deviations were halved, the zero-percent error marked moved beyond the confines of the 95% confidence interval.

Implications of Sensitivity Results

The NEPP sensitivity studies give greater insight into the results shown in Figures 4-4 & 4-5. These distributions depicted the modeling error as contained within the modeling uncertainty at both takeoff and cruise. Although this conclusion applies to all of the example engines, the zero-percent error mark was only marginally within the confines of the 95% confidence interval for the GE90 and CFM56. Moreover, small perturbations to the selection of the means of the input distributions can have a large effect on the mean of the output distribution. Similarly, the variances of the adiabatic efficiencies and bleed flow into the HPT can shape the output distribution. This suggests that NEPP is an accurate engine cycle deck, if supplied with reasonable inputs. The newer and higher BPR engines, the GE90 and CFM56, have complex bleed flow schedules and advanced components. Successfully modeling these nuances in a NEPP input file is difficult. Great care should therefore be taken when modeling future aircraft and engines with NEPP. This is discussed further in Section 4.3.5 below.

4.3.4   Propagation of Uncertainty to EDS Level

With the extent of NEPP uncertainty and its sources understood, attention was turned to the final step of the assessment procedure. The variation in takeoff and cruise TSFC can lead to variable range for a fixed fuel volume or variable fuel burn for a fixed range of an aircraft. A 777-200ER size airframe, with GE90-90B engines, was modeled in EDS then optimized for minimum fuel burn over a 6000 nm mission. The resulting aircraft geometry and aerodynamic performance statistics were combined with the TSFC values from the Monte Carlo simulation for the GE90-90B to generate cruise range and fuel burn distributions, as shown in Figure 4-10. The TSFC distributions resembled normal distributions, but the range and fuel distributions more closely resemble log-normal distributions. This is can be explained with a simple model, the Breguet range equation, which has a logarithm of the weight ratio,

$$R = \frac{V}{SFC} \frac{L}{D} \ln \frac{W_i}{W_f}$$

(a) Range   (b) Fuel burn
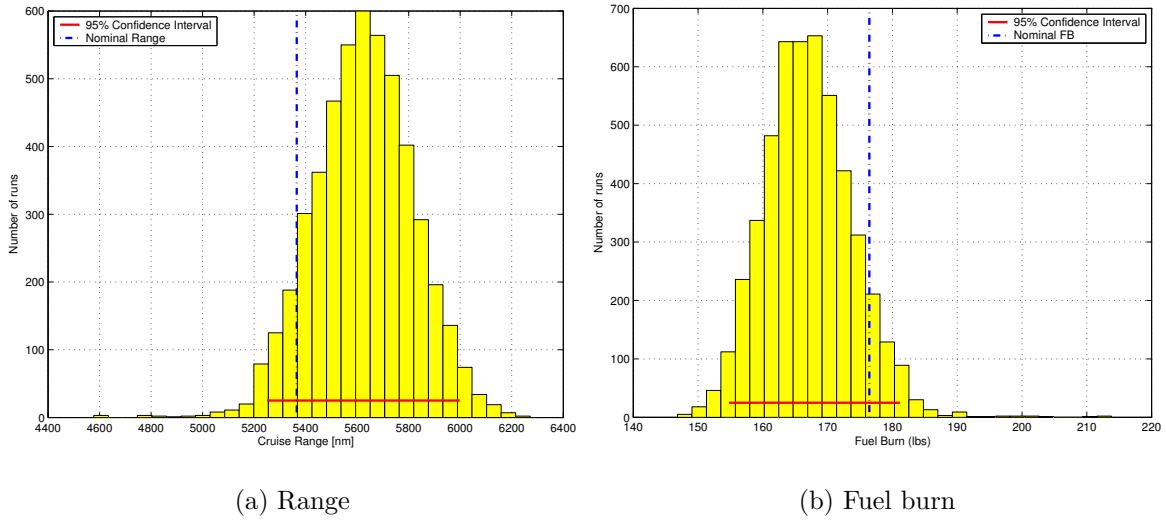
Figure 4-10: Propagation of uncertainty in cruise TSFC for the GE90 through the Caffe framework. Nominal line indicates the performance if an actual GE90-90B were placed on the example aircraft.

where V is the flight speed, L/D is the lift-to-drag ratio, W_i is the initial cruise weight and W_f is the final cruise weight.

The 95% confidence interval for the fuel burn in Figure 4-10b spans 26,404 lbs. While this might seem excessive, the coefficient of variation, CV (ratio of standard deviation to the mean), for this distribution is only 4.1%, which is quite reasonable considering the average CV of the inputs was 11%. Furthermore, fuel costs are typically around 8% of the total operating costs of aircraft [28]. Thus, this variability in fuel burn would only be a small fraction of the cumulative variability of TOC.

It is important to note that this uncertainty in range or fuel burn is generated by NEPP only and does not contain the uncertainty contributions of other modules. Moreover, even though the CV for the cruise TSFC error of the GE90 was 73%, the CV for fuel burn was only 4.1%. Thus, the numerous uncertainties that begin at the module input level become diluted as they are propagated to the system level. It is quite possible that when the uncertainty contributions from other modules are considered as well, the variance in fuel burn will be further reduced.

4.3.5   Summary and Conclusions

To summarize, a probabilistic model assessment methodology was motivated, presented and explained. This methodology was applied to the EDS engine cycle deck,

NEPP, for takeoff and cruise TSFC performance.

NEPP accurately captures the performance of the PW4056 and only marginally captures the performance of the CFM56 and the GE90 at takeoff. The sensitivity studies in Section 4.3.3 show that for the GE90, changes in the input distribution means and standard deviations could shift the output mean and confidence interval away from the zero-percent error mark. Moreover, the engines for which NEPP had modeling difficulty, the CFM56 and GE90, have complex bleed flow schedules, cooling schemes and advanced design methods. These facts lead to the conclusion that NEPP is generally an accurate engine cycle deck if the user is able to supply it with accurate inputs. The selected means for the variables with the largest impact on the output, namely the adiabatic efficiencies and the amount of bleed flow that enters the HPT, for the CFM56 and GE90 most likely deviated slightly from their true values and led to their marginal success.

The results of the NEPP validation study and the propagation of uncertainty to the system level has implications for future studies. Figure 4-9b & 4-8 demonstrate the importance of modeling the input means accurately, especially for the efficiency variables. Consistently under-predicting the input mean by just 1% can shift the output distribution by 3%. Thus, when new aircraft and engines are designed within Caffe, improving the knowledge about the efficiency variables would yield the greatest benefit for reducing the uncertainty of the outputs at both the NEPP and EDS level. Fortunately, as the uncertainty propagates from the module level to the system level, the magnitude of variance goes down. Meaning, although the CV of the inputs was 11% and the CV of cruise TSFC error for the GE90 was 73%, the CV of fuel burn was only 4.1%.

Chapter 5

Exploration of EDS Tradeoffs

5.1 Introduction

This chapter begins to view aircraft performance in the context of the environmental design space. The example case of Section 3.4 generated results along the axes of GTOW and *LTO-NO$_x$*. This chapter extends that concept and demonstrates that there is a tradeoff between the EDS objectives, as shown in Figure 5-1. Often times competition between aircraft performance, which might be GTOW or fuel burn or operating cost, NO_x and noise arise in aircraft design.

5.2 EDS Tradeoffs

The most common method by which to view tradeoffs between two or more competing objectives is through multi-objective optimization and Pareto fronts. An aircraft designed explicitly for minimum NO_x emissions would look different from an aircraft
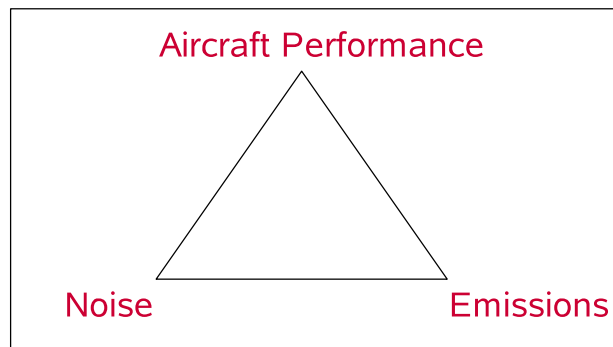
Figure 5-1: Competing objectives within EDS.
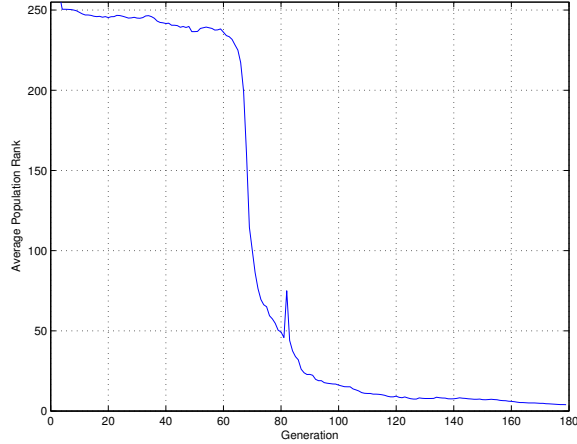
Figure 5-2: Average population rank vs. GA generation in multi-objective optimizations for cumulative EPNL vs. $LTO\text{-}NO_x$.

designed chiefly for minimum noise, and both would contrast with a design for simultaneous minimization of NO_x and noise together. A Pareto front depicts these scenarios and everything in between as a curve between the axes of competing objectives.

5.2.1   Approach for 2-Objective Optimizations

The three Pareto fronts in Figures 5-3–5-4 were the results of a multi-objective GA optimization with a population size of 500 and a mutation rate of 3%. The optimizations were run until the Pareto front no longer moved in the design space, which corresponded to an average population rank near 4. The optimization for cumulative EPNL and $LTO\text{-}NO_x$ started with a random seeding of the initial population. Randomly populating the design space initialized many infeasible designs and the optimizer was forced to seek out feasible regions of the design space. To save computational time, the other two optimizations were started with initial populations of previously determined feasible designs. The convergence history of the cumulative EPNL and $LTO\text{-}NO_x$ optimization is shown in Figure 5-2. To reach the convergence criterion of average population rank of 4 required over 175 GA generations.

5.2.2   Noise vs. NO_x

For the same aircraft type and constraints as used in the example case study in Section 3.4, a multi-objective optimization between cumulative EPNL and $LTO\text{-}NO_x$ was performed. The resulting Pareto front, depicted in Figure 5-3, shows a smooth tradeoff between the two environmental metrics. All of the points shown in Figure 5-3 are

64
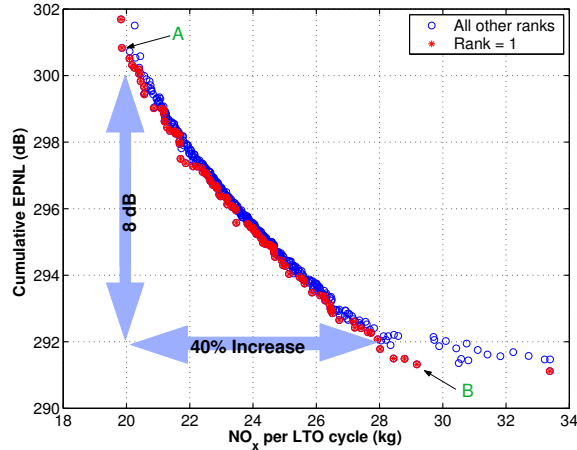
Figure 5-3: Pareto front between cumulative EPNL and $LTO\text{-}NO_x$. Points A and B indicate the points of comparison in Table 5.1.

unique designs. While all points satisfy the constraints that bound the optimization, each is a different set of design variables. The red, asterisk points are denoted as *Rank-1*, or non-dominated designs. Non-dominated designs imply that there is no other point that performs better in both noise and NO_x. For a given Rank-1 point, any other design that performs better in noise would perform worse in NO_x, or vice-versa.

The Pareto front in Figure 5-3 varies from low $LTO\text{-}NO_x$ designs to low noise designs. It is interesting to interrogate the plot and reveal the changes in the design variables from one extreme to the other. The far ends of the Pareto front in Figure 5-3 are labelled by A (low NO_x) and B (low noise). The design variables for these points are listed in Table 5.1. For a low noise design, the optimizer chose a large BPR engine of 12.08, with a low FPR, to reduce the fan noise component. To drive this large fan, the engine core required a high OPR. However, the high OPR led to higher temperatures and pressures at the combustor inlet, leading towards larger NO_x production. In contrast, for a low $LTO\text{-}NO_x$ design, the low temperatures and pressures and the combustor inlet translated to a smaller OPR, for which the engine could only support a smaller BPR of 8.45.

Just as the extrema of the Pareto front in Figure 5-3 contain insight into the environmental tradeoffs, so too does the slope of the curve. The block arrows indicate that at the design space envelope, for an 8 dB reduction in cumulative EPNL, there is a corresponding increase in $LTO\text{-}NO_x$ of 8 kg. Figure 5-3 could supply a regulatory or design decision maker with the information necessary to weigh the trades. Would an exchange of 8 dB in cumulative noise for a 40% increase in $LTO\text{-}NO_x$ be a worthwhile

Table 5.1: Comparison of design variables for low noise and low NO_x designs (points A and B) from Figure 5-3.

	Variable	Point A	Point B
Aircraft	GTOW (lbs)	452,531	417,551
	S_{ref} (ft^2)	3,980	3,416
	AR	7.17	8.13
	Sweep (deg)	31.4	30.2
Engine	SLS Thrust (lbs)	79,706	79,802
	BPR	8.45	12.08
	T_{t4} $(°R)$	3,084	3,230
	OPR	42.99	58.49
Obj	Cumulative EPNL (dB)	300.71	291.77
	LTO-NO_x (kg)	21.326	32.715

tradeoff from an environmental perspective? From a business perspective? Without a common metric or basis of comparison, it is difficult to assess the benefit or value of any trades. Section 5.2.4 offers a couple means of comparison that might enable these trades.

5.2.3 GTOW vs. NO_x and GTOW vs. Noise

Figure 5-1 demonstrates three combinations of tradeoffs between aircraft performance, emissions and noise. Figure 5-3 depicts only one combination of EDS tradeoffs. The remaining combinations are shown in Figure 5-4. In these Pareto fronts, GTOW serves as a surrogate for aircraft performance and cost as many aircraft design projects seek to minimize GTOW. Not only do these plots demonstrate the tradeoffs between the competing objectives, but the scalings of the Pareto fronts in Figure 5-4a and 5-4b are quite different. In Figure 5-4a, the front relates 1 kg of LTO-NO_x to 7,500 lbs of GTOW. In Figure 5-4b, the Pareto front trades 1 dB of cumulative EPNL to 5,500 lbs of GTOW. While making these trades and comparing the different curves is again difficult, it provides designers or regulators with the information to make decisions.

5.2.4 Noise vs. NO_x vs. Cost

The final step in illustrating the tradeoffs within EDS after illustrating the Pareto fronts for the objectives in Figure 5-1 is a 3-objective optimization between all competing objectives. This was also accomplished with the use of a multi-objective GA. Instead of a curve, the 3-D Pareto front is a surface defined by the Rank-1 points. To shape this surface, a population size of 2200 was used so that when the optimization neared convergence, there would be at least 500 Rank-1 points. The 3-objective opti-

(a) GTOW and $LTO\text{-}NO_x$ (b) GTOW and cumulative EPNL
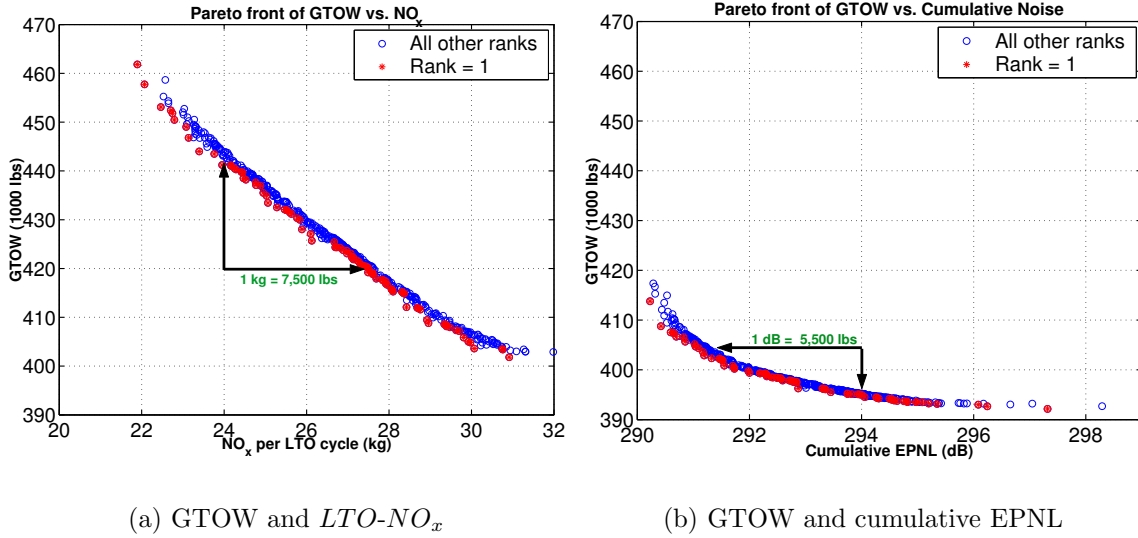
Figure 5-4: Pareto fronts of EDS tradeoffs. GTOW serves as a surrogate for aircraft performance and cost.

mization was run for 214 generations until the average rank of the population dropped below 3 and there were 567 Rank-1 points in the population. The convergence criterion used for the 3-objective optimization was more stringent than the criterion for the 2-objective optimizations because many more Rank-1 points were required to define the surface. The optimization history is shown in Figure 5-5a with a logarithmic scaling of the y-axis to account for the significant changes in average rank.

The 3-objective optimization between cumulative EPNL, $LTO\text{-}NO_x$ and relative cost is depicted in Figure 5-5b. The relative cost metric is an approximation of the cost per seat-mile, divided by the lowest cost point. It is therefore a relative summation of direct and indirect operating cost. The cost model, originally developed by the Air Transportation Association in 1967, includes contribution from crew salaries, fuel consumption, maintenance, depreciation and block time. The coefficients and cost estimates have been revised periodically to account for inflation, but are nevertheless still outdated. The clustering of points and the interpolation of data between them induces some numerical artifacts in the plot, so small contour islands and detailed features in Figure 5-5b should not be interpreted rigorously. Nevertheless, the general trends and qualitative information are the important details communicated in this plot. For instance, the higher cost designs are those at the forefront of the low noise, low NO_x region, with more emphasis on lower NO_x than lower noise.

Figure 5-5b might offer a mechanism by which to make the trade for cumulative EPNL and $LTO\text{-}NO_x$. This 3-objective optimization enables noise and emissions to

(a) Average population rank vs. GA generation

(b) 3-obj Pareto front with 567 Rank-1 points
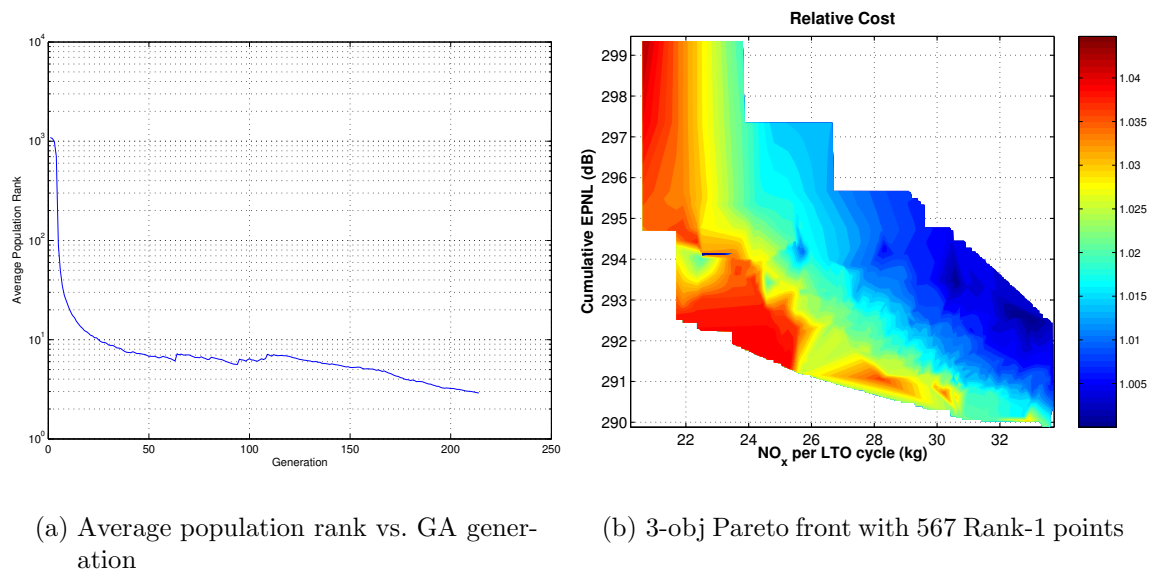
Figure 5-5: Optimization for cumulative EPNL vs. $LTO\text{-}NO_x$ vs. relative cost.

be traded along iso-cost contours. Meaning, cumulative EPNL and $LTO\text{-}NO_x$ could be exchanged in a proportion that does not incur any additional cost to the airline operators. Another method by which one might compare environmental metrics on common ground is through the social valuation of environmental impacts. Social valuations focus on the costs incurred by society from environmental disturbances. For instance, older, louder aircraft can be considered a nuisance in neighborhoods surrounding airports. Community activists might demand sound insulation installed in those homes and the neighborhood property value might be devalued. Similarly, aircraft $LTO\text{-}NO_x$ emissions contribute to the local air quality and can affect the health of city residents. The EPA also monitors local air quality and can levy fines if standards are not met. All of these impacts incur a cost to society that would not ordinarily be accounted for by airline operating costs or the cost estimation used for Figure 5-5b. Arriving at social valuations for environmental impacts is not only a difficult modeling task, but also has many political implications. It is a subject of future research and was not available for inclusion in this thesis.

5.3 Technology Tradeoffs in EDS

To improve the environmental performance of aircraft, or to maintain compliance with future regulations, there are a number of technologies in development to ameliorate the noise and emissions output of aircraft. These technologies often focus to mitigate
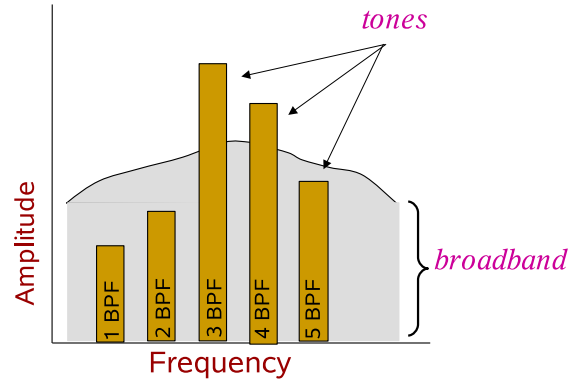
Figure 5-6: Diagram of fan noise sources across frequencies.

the contribution of a single noise or emissions source. In so doing, however, future technologies are often not considered in the system-level trade space of EDS. This section scrutinizes one such technology, fan trailing edge blowing, in the EDS context.

Without years of engineering demonstration or experience, new technologies are not well understood and have high uncertainty. New technologies remain unperfected, in development and often far from being flight tested. Therefore, their performance, when installed on aircraft, can only be estimated. Analytical, computational and experimental demonstrations of the technology all have their limitations in predicting performance. Thus, in the presence of this technological uncertainty, a probabilistic analysis is the most appropriate approach in modeling the performance of new technologies. A probabilistic analysis does not discard or ignore the technological uncertainty, but rather explores its implications on performance.

5.3.1 Fan Trailing Edge Blowing

Noise generated from engine fans can generally be classified as either *broadband* or *tonal* noise. Broadband noise pervades all frequencies in the spectrum and is generated from the turbomachinery and high tip speeds of the fan. Tone noise is a product of the interactions between the wake of the fan rotor and the stator behind it [21]. An illustration of broadband and tonal noise is shown in Figure 5-6. Behind the rotor is a velocity defect in the wake. When that velocity defect impinges on the stator a pure tone noise is generated. That pure tone is generated at a frequency corresponding to a multiple of the blade passing frequency (BPF).

Fan trailing edge blowing is an innovative technique to reduce broadband and tonal fan noise. By ejecting air from the trailing edge of the fan, the mass/momentum defect of the wake is nearly filled in. This can significantly reduce the rotor wake-

stator interaction noise. Experimental results suggest that the tonal noise reduction from this technology could be as much as 10 dB [9].

Additional experimental investigations at NASA Glenn on the Active Noise Control Fan have furthered the development of the technology [44]. Greater effort was made to characterize the performance of the technology, as well as to seek an optimal blowing ratio, or the percentage mass flow ejected at the trailing edge.

Although the fan trailing edge blowing shows significant promise for noise reduction, it also diverts air from the core engine flow. The ejected air must come from an additional bleed from the compressor. This additional bleed degrades the efficiency and thrust output of the engine. Moreover, the infrastructure in the engine necessary to carry mass flow from the compressor and into the hollow fan blades carries a weight penalty. This weight penalty impacts the performance of the entire aircraft system. Thus, the fan trailing edge blowing is a candidate for a tradeoff study between noise reduction and fuel burn.

5.3.2   Simplified Model

All of the investigators into the fan trailing edge blowing technology identified the blowing ratio as the key driver for noise reduction performance [9, 44]. If the blowing ratio is too small, rotor wake-stator interaction noise remains strong. If the blowing ratio is too large, then the wake is over filled and interaction noise returns. The optimal blowing ratio should scale with the FPR, which is inversely proportional to BPR. A smaller FPR implies a smaller velocity deficit in the wake to fill in. Sutliff and Brookfield found an optimal blowing ratio near 1.8% in their experimental studies, but Prasad showed optimal blowing ratios near 1.2% for a 12 BPR fan [46]. Since the baseline aircraft of comparison had an engine BPR near 10, 1.2% was selected as the optimal blowing ratio.

Experimental results done by Sutliff et al. at NASA Glenn were used as the basis for the noise reduction model. Empirical measurements for the first seven harmonics were made for an engine test rig with the fan trailing edge blowing technology, where the harmonics are integer multiples of the blade passing frequency (BPF). Results showed that for the optimal blowing ratio the harmonic tone noise was reduced by approximately 8 dB. However, at blowing ratios below or above the optimum value, the tone noise reduction was less.

Noise Impact

The fan trailing edge blowing noise reduction implementation in the computational framework reflected the experimental results at NASA Glenn. The fan tone noise calculations were isolated as a separate component within ANOPP. These tone har-

monics were suppressed by $8\,\mathrm{dB}$, and then propagated to the observer with the other noise sources. This approach successfully accounted for the shift in perceived harmonic frequencies through atmospheric attenuation. Finally, since the technology has a larger impact on the BPF tones than the broadband noise component and since empirical results on the broadband impact are still forthcoming, the fan broadband noise calculation was not modified in any way.

Impact on Engine Cycle

For the impact of the cycle, an additional bleed flow was modeled from the low pressure compressor to the fan. This effect approximated the detriment the fan trailing edge blowing technology would have on overall engine efficiency and thrust output. The addition of another secondary flowpath would have a weight impact as well. Weight breakdowns of engine components, including secondary flow, were examined from the NASA WATE code (a program designed to estimate engine weight and flowpath geometry from cycle and material specifications). These weight breakdowns suggested that a penalty of 4% would appropriately capture the augmented engine weight.

There was one final effect that the fan trailing edge blowing technology would have upon the engine cycle. As the bleed flow from the compressor travels along the fan disk from the hub to the tip, work is done on the bleed flow since it is in a rotating reference frame. The fan and bleed flow act like a centrifugal compressor in this way. Therefore, there is an effective increase in BPR of the engine. More flow is being worked on by the fan, so it is as though more mass flow were entering the fan at the inlet.

The fan trailing edge bleed flow was assumed to be inviscid, incompressible and travel within the blade as seen in Figure 5-7 with no change in entropy. If the toal amount of bleed flow is denoted by, m_b, and the hub radius is assumed to be zero, then the mass flow up to a point, r can be written as,

$$\dot{m} = \dot{m}_b \frac{r}{r_t}$$

where r_t is the tip radius of the fan. Differentiating yields,

$$d\dot{m} = \frac{\dot{m}_b}{r_t} dr \tag{5.1}$$

The work done by a differential fluid element through an ideal centrifugal compressor from $r = 0$ to r is the rate of change of angular momentum,

$$d\dot{W} = (r\omega)^2 \, d\dot{m} \tag{5.2}$$

71
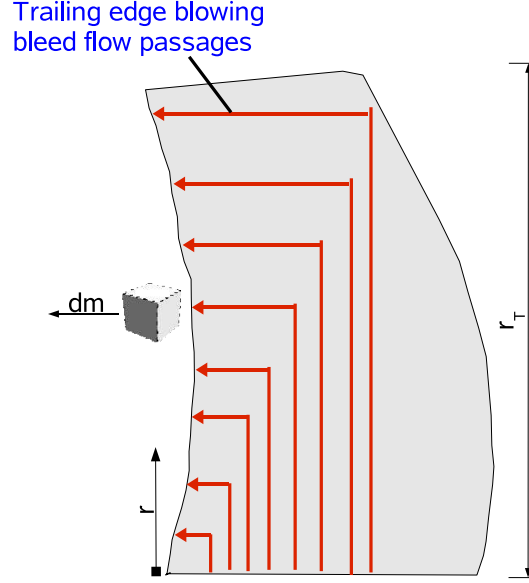
Figure 5-7: Assumed flowpath of fan trailing edge blowing bleed flow through the fan blade.

substituting in Equation 5.1 and integrating yields,

$$\dot{W}_b = \int_0^{r_t} (r\omega)^2 \frac{\dot{m}_b}{r_t} dr = \frac{1}{3}\dot{m}_b (r_t\omega)^2 \tag{5.3}$$

Similarly, for the airflow that enters the fan face, the amount of work done is related to the rate of change of angular momentum,

$$\dot{W} = \dot{m}_i r\omega (v_{\theta_2} - v_{\theta_1}) \tag{5.4}$$

where $\dot{m}_i$ is the total inlet mass flow and v_θ is the swirl velocity. The diffusion factor, D, relates the velocity components before and after a compressor rotor as a non-dimensional measure of flow turning,

$$D = 1 - \frac{V_2'}{V_1'} + \frac{|v_{\theta_2} - v_{\theta_1}|}{2\sigma V_1'}$$

where V' is the velocity magnitude in the rotating frame and σ is the blade solidity, which is assumed to be unity. At the fan face, it assumed that the incoming flow has no swirl, $v_{\theta_1} = 0$. If the diffusion factor is assumed to be 0.3 and the axial velocity assumed to be 75% of the rotor tangential velocity, then it can be shown that

72

$v_{\theta_2} \approx 0.3r\omega$. Substituting back into Equation 5.4,

$$\dot{W}_f = \frac{3}{10}\dot{m}_i\left(r\omega\right)^2$$

Under a meanline assumption, the radius is assumed to be the average of the hub and tip radius. Assuming the hub radius is zero, $r = r_t/2$ and the work becomes

$$\dot{W}_f = \frac{3}{40}\dot{m}_i\left(r\omega\right)^2 \tag{5.5}$$

The BPR, α, is defined to be the ratio of mass flow through the fan to the mass flow through the engine core,

$$\alpha = \frac{\dot{m}_f}{\dot{m}_c}$$

where $\dot{m}_i = \dot{m}_f + \dot{m}_c$. Thus, Equation 5.5 can be rewritten as,

$$\dot{W}_f = \frac{3}{40}\left(r_t\omega\right)^2\dot{m}_c\left(\alpha+1\right) \tag{5.6}$$

Similar to the BPR, the blowing ratio, β, is defined as the ratio of bleed flow air ejected out the trailing edge of the fans to the total incoming mass flow,

$$\beta = \frac{\dot{m}_b}{\dot{m}_i}$$

with which Equation 5.3 can be rewritten as,

$$\dot{W}_b = \frac{1}{3}\beta\dot{m}_c\left(\alpha+1\right)\left(r_t\omega\right)^2 \tag{5.7}$$

Finally, the effective BPR, α', is the BPR at which the same amount of equivalent work is done but without the presence of the fan trailing edge blowing technology,

$$
\begin{aligned}
\dot{W}_f' &= \dot{W}_f + \dot{W}_b \\
\frac{3}{40}\left(r_t\omega\right)^2\dot{m}_c\left(\alpha'+1\right) &= \frac{3}{40}\left(r_t\omega\right)^2\dot{m}_c\left(\alpha+1\right) + \frac{1}{3}\beta\dot{m}_c\left(\alpha+1\right)\left(r_t\omega\right)^2 \\
\frac{3}{40}\left(\alpha'+1\right) &= \frac{3}{40}\left(\alpha+1\right) + \frac{1}{3}\beta\left(\alpha+1\right) \\
\alpha' &= \alpha + \frac{40}{9}\beta\left(\alpha+1\right)
\end{aligned}
$$

For an engine with a BPR of 10 and a blowing ratio of 1.2%, the effective BPR would be, $\alpha' = 10.587$.

Table 5.2: Comparison of baseline aircraft with and without the fan trailing edge blowing technology. For aircraft with the technology a subscript of $+1.5\sigma$ indicates the robust design for variability. An asterisk on the objectives implies that they are the metrics for the robust design evaluated at the nominal blowing and weight penalty ratio of 1.2% and 4%, respectively.

	Variable	Without	With	With$_{+1.5\sigma}$
Wing	GTOW (lbs)	341,676	355,073	363,380
	S_{ref} (ft^2)	2,639	2,576	2,669
	AR	10.28	11.38	11.58
	t/c	0.129	0.129	0.130
	Sweep (deg)	34.2	34.1	34.9
Engine	SLS Thrust (lbs)	73,007	78,850	80,266
	BPR	10.33	9.46	9.02
	T_{t4} ($^\circ R$)	3,293	3,296	3,300
	OPR	59.97	60.00	60.00
	FPR	1.491	1.442	1.459
	CPR	27.30	39.98	39.25
	Blowing ratio	0.0	0.012	0.0135
	Weight penalty ratio	0.0	0.04	0.0505
Objectives	Fuel burn (lbs)	105,304	105,898	108,269*
	Flyover (dB)	89.56	77.38	77.65*
	LTO-NO_x (kg)	33.34	35.82	37.01*

5.3.3 Probabilistic Tradeoff Analysis Approach

To initiate the tradeoff study for the fan trailing edge blowing technology, two baseline aircraft were created. The baseline airframes were of a 767-300ER size aircraft (275 passengers) with a 6000 nm cruise range, the same aircraft type as used above in Section 3.4. Both aircraft were optimized for minimum mission fuel burn using the simplex optimizer. One of the aircraft was modeled with the fan trailing edge blowing at the optimal blowing ratio and the other aircraft was optimized without the technology. The applicable design variables for these two aircraft are listed in Table 5.2. The optimization for the aircraft with the technology also included a requirement that both the flyover and cumulative EPNL metric be at least 5 dB below that of the aircraft without the technology. Although the final design in Table 5.2 depicts significant margin for this additional constraint, it helped to steer the optimizer in the right search direction.

Once the baseline aircraft were set, a Monte Carlo simulation was performed. This probabilistic analysis accounted for the high level of uncertainty associated with new technologies. A listing of the stochastic variables used in the simulations, as well as their probabilistic parameters is found in Table 5.3. Each input was considered

Table 5.3: Stochastic variables and their normal distribution parameters for the fan trailing edge blowing technology model.

Variable	Mean	Std Dev
Blowing ratio	0.012	0.001
Noise reduction	8 dB	2.6 dB
Weight penalty ratio	0.04	0.007

normally distributed about its mean. The Monte Carlo simulation randomly sampled these input distributions 5000 times to generate the output distributions. The output distributions, as well as their associated confidence intervals, were used for tradeoff assessment and comparison.

5.3.4   Results

When the variables associated with the technology (the blowing ratio and noise reduction) are considered stochastic, important robustness lessons are revealed. An optimized solution implies that the design vector abuts constraint boundaries. The small perturbations to the stochastic variables in the Monte Carlo simulation inevitably cause some of the designs to cross these boundaries. For the Monte Carlo simulation of the fan trailing edge blowing technology, 66% of all iterations violated constraints. Of the three stochastic variables in Table 5.3, only the blowing ratio and weight penalty ratio could impact aircraft performance. Meaning, the perturbations to the stochastic variables degraded the efficiency of the aircraft enough to decrease the performance below a critical design constraint. A higher engine weight led to a higher zero-fuel weight of the aircraft. Similarly, a higher blowing ratio degraded the fuel efficiency of the engine. The combination of these variables leading to feasible or constraint-violated designs is evident in Figure 5-8a. Additionally, of the constraint violations, 58% of them were violations of the cruise range constraint. These designs were concentrated in the upper left quadrant of Figure 5-8a, where the weight penalty ratio was above its mean value but the blowing ratio was below. Range performance below the design point of 6,000 nm could be accepted as a drawback or tradeoff of incorporating the fan trailing edge blowing technology. However, there were also takeoff field length constraint violations, which would vitiate the design completely. These takeoff field length violations are indicated by the black hash points in Figure 5-8a and located in the right-hand side of the plot. More Carlo iterations with the blowing ratio above its nominal value led to infeasible designs, which numbered to be 42% of the constraint violations and 28% of all iterations total. The feasible designs in Figure 5-8a are clearly concentrated in the quadrant where the blowing ratio and weight penalty ratio values are below their mean values.
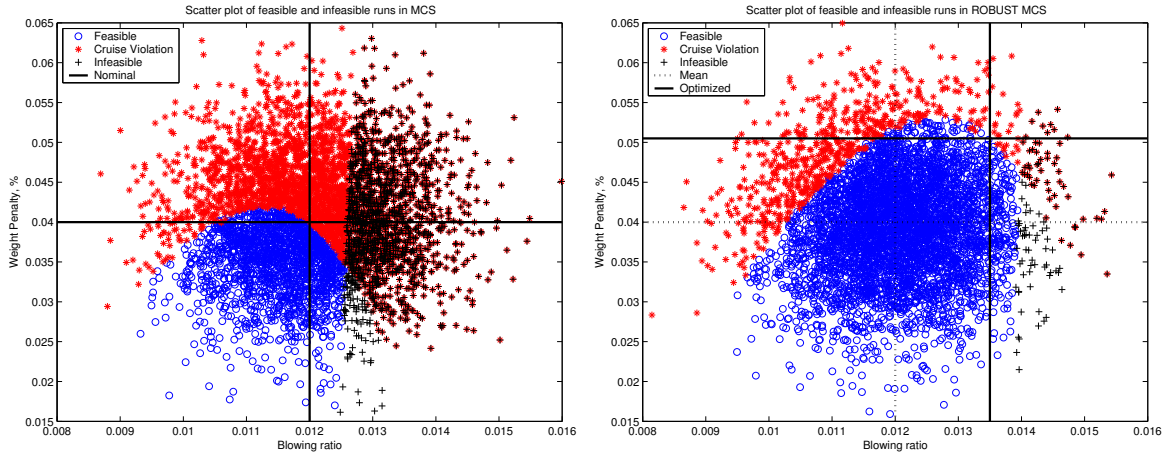
(a) Initial MC simulation with equal optimized and mean values

(b) Design for robustness approach with optimized values 1.5σ above the mean values

Figure 5-8: Scatter plots of feasible and constraint-violated designs in Monte Carlo simulations.

Design for Robustness

The scatter plot in Figure 5-8a demonstrates the poor robustness of the aircraft with fan trailing edge blowing. Design for stability and robustness of an engine with this technology must account for variability. An improved design methodology was proposed and executed to enhance the variability tolerance of the aircraft with the technology. First, the optimization for minimum mission fuel burn was performed with a higher baseline blowing ratio of 0.0135 and a weight penalty ratio of 0.0505. These values were chosen because they were one and a half standard deviations above the Monte Carlo mean values. The applicable design variables from this optimization are compared to the first two baseline aircraft in Table 5.2. Although this third baseline aircraft was optimized at a blowing ratio of 0.0135 and weight penalty ratio of 0.0505, it was run in a Monte Carlo simulation with a mean blowing ratio of 0.012 and mean weight penalty ratio of 0.04, just as before. This was therefore the design mechanism by which the engine could tolerate the variability that it might encounter.

The improved robustness of designing for a higher blowing ratio and weight penalty ratio is evident in the scatter plot of Figure 5-8b. Whereas initially 66% of all runs violated constraints, in the robust design Monte Carlo simulation only 15% of the iterations violated constraints. Furthermore, only 2% of all Monte Carlo iterations violated the takeoff field length constraint and vitiated the design. This corroborates the robust design approach as a refined methodology for incorporating the fan trailing

76

edge blowing technology into an aircraft-engine system.

Tradeoffs

The robust design in Table 5.2 is clearly the preferred design and is used as the mechanism of comparison against the aircraft without the technology. The price of robustness, comparing the non-robust technology design to the robust design, is an additional fuel burn and LTO-NO_x penalty of 2.2% and 3.3%, respectively. The design variables in Table 5.2 are scrutinized to understand the system-level impact of the technology.

It is apparent from Table 5.2 that the aircraft with the technology cannot support as high of a BPR as the aircraft without the technology. To overcome this shortfall and maintain cruise range, the optimizer incremented the aspect ratio of the wing to reduce the induced drag. This modification required greater structural supports and made the entire aircraft heavier, which necessitated a higher thrust engine as well. With the enlarged thrust class and smaller BPR, the technology aircraft also had increased core mass flow, $\dot{m}_c$. In fact, the core mass flow for the technology aircraft was 295 lb/s compared to only 240 lb/s for the baseline aircraft without the technology. This additional mass flow required greater fuel flow to meet the target combustor exit temperature, T_{t4}. The higher fuel flow rate explains the 2.8% degradation in mission fuel burn and the 11.0% degradation in LTO-NO_x.

Although the fan trailing edge blowing effected significant improvement in the fly-over noise metric, it came with a fuel burn and LTO-NO_x price. It offers a 11.91 dB reduction in flyover noise and a 14.60 dB reduction in cumulative EPNL for 2.8% increase in fuel burn and 11.0% increase in LTO-NO_x. As discussed above, the quantification of the tradeoffs enables a designer or regulator to make decisions. Perhaps the use of social valuations or the iso-cost contours in Figure 5-5b or a combination of the two concepts could contribute to the decision making process. Nevertheless, examining this technology probabilistically revealed robust design implications. Moreover, assessing the technology in the context of EDS brought to light the drawbacks associated with aircraft performance and emissions.

5.4   Summary

This chapter has depicted the tradeoffs between the competing EDS objectives and characterized their relationships. These tradeoffs provide a designer or regulator with the information required for decision making. In the context of these tradeoffs, the fan trailing edge blowing technology was examined in the EDS framework. A probabilistic approach was once again employed and proved its usefulness by suggesting robust design methodology improvements for the technology. On a system level, the

technology offers attractive noise reduction benefits at the cost of detriments to fuel burn and $LTO\text{-}NO_x$.

Chapter 6

Conclusions and Future Work

6.1 Conclusions

This thesis has broached the context of the environmental design space for analysis of commercial aircraft. EDS implies exploring the trades in aircraft design between traditional performance metrics, such as fuel burn, range or cost versus environmental performance metrics, such as $LTO\text{-}NO_x$ and cumulative EPNL simultaneously. This perspective becomes increasingly necessary as new aircraft continue to push the design space envelope and regulations become more stringent. While some preliminary research has been performed in this area at Georgia Tech and others, this thesis makes several important contributions.

Probabilistic assessment methodology When working with complex system design tools, such as Caffe, understanding the uncertainties and errors at the module and system level is essential. Thus, a probabilistic module assessment methodology was devised and includes steps starting from the selection of stochastic variables through the propagation of module uncertainty to the system level. This generic methodology was applied to the Caffe engine cycle deck module, the NASA Engine Performance Program. The methodology successfully identified the key drivers of NEPP uncertainty and determined that the modeling error was overshadowed by the modeling uncertainty. It also signalled that ascertaining specific engine design characteristics is a crucial step to appropriately capturing engine performance. Moreover, uncertainties at the module input level dissipate when propagated to the system level.

System level EDS study of fan trailing edge blowing Fan trailing edge blowing is a future noise reduction technology aimed at ameliorating the fan rotor-stator interaction tone and broadband noise. Ejecting bleed air out the trailing edge of the fan blades fills in the velocity defect in the wake. The bleed air

flow, however, degrades engine performance and augments weight. This thesis provides both a probabilistic, system-level view of the fan trailing edge blowing technology and also examines it through an EDS lens. Once the technology was successfully modeled and incorporated in Caffe, a Monte Carlo simulation revealed poor robustness performance of the initial design. A robust design procedure was proposed and executed, which allowed for tradeoffs to be made. The fan trailing edge blowing technology offers a cumulative EPNL savings of 14.6 dB, but at the cost of a 2.8% increase in fuel burn and a 11.0% increase in $LTO\text{-}NO_x$.

The Pareto fronts demonstrating EDS tradeoffs represent another contribution of this thesis that was made in collaboration with Antoine and Kroo [3]. Pareto fronts are a standard projection of competing objectives in a multi-objective optimization. Caffe, with its integrated aircraft-engine design capabilities, facilitated the depiction of the EDS metrics as Pareto fronts. While system level trades of fuel burn vs. emissions or cost vs. noise are made constantly by aircraft designers, these tradeoffs are characterized here through multi-objective genetic algorithms. Presenting the Pareto fronts is not only communicative in terms of depicting the tradeoffs, but also quantifies the relationship between EDS metrics. Meaning, an 8 dB reduction in cumulative EPNL is coupled with an 8 kg increase in $LTO\text{-}NO_x$ for a given aircraft. However, evaluating these ratios or trades in terms of a common cost unit remains a difficult task and a subject of future investigation.

6.2   Future Work

Although this thesis provides a foundation for Caffe assessment and EDS investigations, the work can be extended and improved in a number of different facets.

The probabilistic assessment methodology was devised to be a generic algorithm that could be applied to any module sub-component of a complex, system design tool. To date, this methodology has only been applied to NEPP. To thoroughly and rigorously assess the EDS framework, this methodology must be executed on the remaining modules. This will not only provide an assessment and uncertainty estimate of each module, but will facilitate a more rigorous estimation of system-level metrics. Meaning, when a probabilistic assessment of each module is complete, the uncertainty can be propagated to the EDS level, just as was done for NEPP. Only then will system-level EDS metrics be understood well enough to provide an estimate of comprehensive uncertainty for a single aircraft. Finally, EDS metrics for a variety of aircraft can be rolled up to the fleet level, which is the context where airline operations and regulatory decisions often reside.

A system-level assessment of Caffe should do more than roll-up the module input uncertainties. A deterministic, example case study in Caffe should be compared to other existing, perhaps proprietary, tools. A companion EDS study for comparison would give additional confidence to the use of Caffe as an integrated aircraft-engine design tool. One issue that must be addressed in the course of this type of study is a statement of how good Caffe, or any system design tool, has to be. Meaning, acceptable levels of error and uncertainty must be specified. Once those standards are established, it would be possible to state, with $X\%$ confidence that Caffe can accurately predict fuel burn or $LTO\text{-}NO_x$ or another metric within $Y\%$ error.

The application of the probabilistic assessment methodology to NEPP identified some areas of improvement for a Caffe engine cycle deck. The results pointed to necessary improvements in the detail of the NEPP inputs to capture advanced engines, as well as uncertainty reduction of the inputs. These shortcomings, along with NEPP's poor usability, suggest that another engine cycle deck might be more appropriate. The NASA Numerical Propulsion System Simulation (NPSS) is one such candidate replacement. NPSS has already been adopted by Pratt & Whitney as a piece of their preliminary design tool and is extremely modular and flexible. Additional information and familiarization of NPSS is required before it can replace NEPP.

The Pareto fronts in Chapter 5 depict and quantify the tradeoffs between the various EDS metrics. Some suggestions were made by which these tradeoffs could be made. For instance, social valuations of environmental impacts could be used as a standard for design or regulatory trades between noise and emissions. Estimating the cost to society from the environmental impact of an aircraft fleet is a subject of future research. This research aims to bookkeep all of the pollutants from aircraft and directly or indirectly link them to a monetary metric, such as change in property values near airports or hospitalization costs from poor air quality. As this research becomes more mature and more widely accepted, it should be incorporated into Caffe. The ability to estimate the social valuations of an aircraft would certainly make the cost model more rigorous.

Similar to the extension of the assessment algorithm to other modules, the modeling of future technologies in the context of EDS should also be extended. While the fan trailing edge blowing technology provided a solid test bed to demonstrate the functionality of the EDS framework, additional technologies should be analyzed. The modeling of new technologies, which often deviate from historical design trends, can be difficult in a semi-empirical tool, such as Caffe. Thus, other technologies that focus on emissions and aircraft performance should be viewed from the EDS perspective to enhance the versatility of Caffe.

Bibliography

[1] Adby, P. R. and Dempster, M. A. H. *Introduction to Optimization Methods.* Chapman and Hall, 1974.

[2] American Institute of Aeronautics and Astronautics. "Guide for the Verification and Validation of Computational Fluid Dynamics Solutions." AIAA Guide G-077-1998, January 1998.

[3] Antoine, Nicolas E. *Aircraft Optimization for Minimal Environmental Impact.* PhD dissertation, Stanford University, Department of Aerospace Engineering, June 2004.

[4] Antoine, Nicolas E. and Kroo, Ilan M. "Aircraft Optimization for Minimumal Environmental Impact." AIAA Paper 2002-5667, September 2002.

[5] Antoine, Nicolas E. and Kroo, Ilan M. "Optimizing Aircraft and Operations for Minimum Noise." AIAA Paper 2002-5868, October 2002.

[6] Baghdasaryan, Lusine, Chen, Wei, Buranathiti, Thaweepat, and Cao, Jian. "Model Validation Via Uncertainty Propagation Using Response Surface Methodologies." DETC2002 DAC-34140, September 2002.

[7] Bertsekas, Dimitri P. *Nonlinear Programming.* Athena Scientific, 1999.

[8] Briceno, Simon I. and Mavris, Dimitri N. "Quiet Supersonic Jet Engine Performance Tradeoff Analysis Using a Response Surface Methodology Approach." SAE Paper 02WAC-120, November 2002.

[9] Brookfield, John M. and Waitz, Ian A. "Trailing-Edge Blowing for Reduction of Turbomachinery Fan Noise." *Journal of Propulsion and Power*, 16(1):57–64, January 2000.

[10] DeLaurentis, Daniel A., Mavris, Dimitri N., Calise, Anthony J., and Schrage, Daniel P. "Generating Dynamic Models Including Uncertainty for Use in Aircraft Conceptual Design." AIAA Paper 97-3590, August 1997.

[11] Department of Defense. "DoD Modeling and Simulation (M&S) Management." DoD Directive Number 5000.59, January 1994.

[12] Fink, M. R. "Airframe Noise Prediction Method." Federal Aviation Administration FAA-RD-77-28, March 1977.

[13] Garzon, Victor E. and Darmofal, David L. "Using Computational Fluid Dynamics in Probabilistic Engineering Design." AIAA Paper 2001-2526, 2001.

[14] Gunston, Bill, editor. *Jane's Aero-Engines.* Sentinel House, 13 edition, 2003.

[15] Hammersley, J. M. and Handscomb, D. C. *Monte Carlo Methods.* Methuen & Co., 1965.

[16] Hazelrigg, George A. "Thoughts on Model Validation for Engineering Design." DETC2003 DTM-48632, September 2003.

[17] Heidmann, M. F. "Interim Prediction Method for Fan and Compressor Source Noise." NASA TM-X-71763, June 1975.

[18] Hough, Joe W. and Weir, Donald S. "Aircraft Noise Prediction Program (ANOPP) Fan Noise Prediction for Small Engines." NASA CR-198300, April 1996.

[19] International Civil Aviation Organization. "Aircraft Engine Exhaust Emissions Databank." http://www.qinetiq.com/aircraft.html, 2003.

[20] Kapper, C. Y. "Validation of Aircraft Noise Prediction Program." NASA CR-159047, June 1979.

[21] Kerrebrock, Jack L. *Aircraft Engines and Gas Turbines.* The MIT Press, 1996.

[22] Kirby, Michelle R. and Mavris, Dimitri N. "Forecasting Technology Uncertainty in Preliminary Aircraft Design." AIAA Paper 1999-5631, October 1999.

[23] Klann, John L. and Snyder, Christopher A. *NEPP Users Manual (NASA Engine Performance Program).* Aeropropulsion Analysis Office, NASA Glenn Research Center, March 1997.

[24] Kontos, K. B., Janardan, B. A., and Gliebe, P. R. "Improved NASA-ANOPP Noise Prediction Computer Code for Advanced Subsonic Propulsion Systems." NASA CR-195480, August 1996.

[25] Kroo, Ilan. "Environmental Design Space (EDS)." Presentation to the FAA, February 2004. unpublished.

[26] Kroo, Ilan M. "An Interactive System for Aircraft Design and Optimization." AIAA paper 92-1190, February 1992.

[27] Lieber, Lysbeth. "Aircraft Noise Prediction Program (ANOPP) Jet Noise Prediction Module, Wing Shielding Module, and System Studies Results." NASA CR-2000-209706, September 2000.

[28] Markish, Jacob. "Valuation Techniques for Commercial Aircraft Program Design." Masters thesis, Massachusetts Institute of Technology, Department of Aeronautics and Astronautics, June 2002.

[29] Mavris, Dimitri N., DeLaurentis, Daniel A., Bandte, Oliver, and Hale, Mark A. "A Stochastic Approach to Multi-disciplinary Aircraft Analysis and Design." AIAA Paper 98-0912, January 1998.

[30] Mavris, Dimitri N., Kirby, Michelle R., and Qiu, Songtao. "Technology Impact Forecasting for a High Speed Civil Transport." SAE Paper 985547, September 1998.

[31] Mavris, Dimitri N., Macsotai, Noel I., and Roth, Bryce. "A Probabilistic Design Methodology for Commerical Aircraft Engine Cycle Selection." AIAA Paper 98-5510, September 1998.

[32] Mavris, Dimitri N., Soban, Danielle S., and Largent, Matthew C. "An Application of a Technology Impact Forecasting (TIF) Method to an Uninhabited Combat Aerial Vehicle." AIAA Paper 1999-5633, October 1999.

[33] Peterson, Arnold P. G. and Ervin E. Gross, Jr. *Handbook of Noise Measurement.* General Radio Co., 1972.

[34] Pierce, Allan D. *Acoustics, An Introduction to Its Physical Principles and Applications.* McGraw-Hill Book Co., 1981.

[35] Roth, Bryce, Graham, Matthew, and Mavris, Dimitri N. "Adaptive Selection of Aircraft Engine Technologies in the Presence of Risk." Technical Report ASME-GT-2002, June 2002.

[36] Roth, Bryce and Mavris, Dimitri N. "A Probabilistic Approach to UCAV Engine Sizing." AIAA Paper 98-3264, July 1998.

[37] Roth, Bryce and Mavris, Dimitri N. "Commerical Engine Architecture Selection in the Presence of Uncertainty and Evolving Requirements." AIAA Paper 2001-1169, September 2001.

[38] Scott, E. Marian. "Uncertainty and Sensitivity Studies of Models of Environmental Systems." In Charnes, J.M., Morrice, D.J., Brunner, D.T., and Swain, J.J., editors, *Proceedings of the Winter Simulation Conference*, pages 255–259, 1996.

[39] Shapiro, S. R. and Caddy, M. J. "NEPCOMP—The Navy Engine Performance Program." ASME Paper 74-GT-83, March 1974.

[40] Shivashankara, Belur N. "Aircraft Noise Prediction Program Validation." NASA CR-159333, 1980.

[41] Society, IEEE Computer. "IEEE Standard for Software Verification and Validation." IEEE Std 1012-1998, March 1998.

[42] Stone, J. R. "Interim Prediction Method for Jet Noise." NASA TM-X-71618, 1974.

[43] Stone, J. R. and Montegani, F. J. "An Improved Prediction Method for the Noise Generated in Flight by Circular Jets." NASA TM-81470, April 1980.

[44] Sutliff, Daniel L., Tweedt, Daniel L., Fite, E. Brian, and Envia, Edmane. "Low-Speed Fan Noise Reduction with Trailing Edge Blowing." AIAA Paper 2002-2492, June 2002.

[45] Thacker, Ben H., Riha, David S., Millwater, Harry R., and Enright, Michael P. "Errors and Uncertainties in Probabilistic Engineering Analysis." AIAA Paper 2001-1239, April 2001.

[46] Topol, David. "NASA T.E.S.T. Task 9 Subtask 2 Final Presentation." Presentation to NASA Glenn, March 2003. unpublished.

[47] Trucano, Rimothy G. "Prediction and Uncertainty in Computational Modeling of Complex Phenomena: A Whitepaper." Sandia Report SAND98-2776, 1998.

[48] Weisstein, Eric W. "Simplex." From MathWorld–A Wolfram Web Resource. http://mathworld.wolfram.com/Simplex.html, 1999.

[49] Younghans, J. L., Luffy, R. J., Bewer, J. T., and Wallace, D. R. "An Integrated Probabilistic Approach to Advanced Commercial Engine Cycle Definition." ISABE Paper 99-7194, September 1999.